

Modified Reverse Osmosis System for Treatment of Produced Waters

Final Technical Progress Report

Principal Author: Robert L. Lee; (505) 835-5408; [lee@nmt.edu](mailto:lee@nmt.edu)

Secondary Author: Junghan Dong; (505) 835-5293; [jhdong@nmt.edu](mailto:jhdong@nmt.edu)

Report Date: June 3, 2004

Reporting Period: September 1, 2000 through February 28, 2004

DOE Award Number: Project No. DE-FC26-00BC15326

Name and Address of Submitting Organization: Petroleum Recovery Research Center  
New Mexico Tech  
801 Leroy Place  
Socorro, New Mexico 87801

## **DISCLAIMER**

This report was prepared as an account of work sponsored by an agency of the United States Government. Neither the United States Government nor any agency thereof, nor any of their employees, make any warranty, expressed or implied, or assumes any legal liability or responsibility for the accuracy, completeness, or usefulness of any information, apparatus, product, or process disclosed, or represents its use would not infringe on privately owned rights. Reference herein to any specific commercial product, process, or service by trade name, trademark, manufacturer, or otherwise does not necessarily constitute or imply its endorsement, recommendation, or favoring by the United States Government or any agency thereof. The views and opinions of authors expressed herein do not necessarily state or reflect those of the United States Government.

## ABSTRACT

This final report of “Modified Reverse Osmosis System for Treatment of Produced Water,” DOE project No. DE-FC26-00BC15326 describes work performed in the third year of the project. Several good results were obtained, which are documented in this report. The compacted bentonite membranes were replaced by supported bentonite membranes, which exhibited the same salt rejection capability. Unfortunately, it also inherited the clay expansion problem due to water invasion into the interlayer spaces of the compacted bentonite membranes. We noted that the supported bentonite membrane developed in the project was the first of its kind reported in the literature. An  $\alpha$ -alumina-supported MFI-type zeolite membrane synthesized by in-situ crystallization was fabricated and tested. Unlike the bentonite clay membranes, the zeolite membranes maintained stability and high salt rejection rate even for a highly saline solution. Actual produced brines from gas and oil fields were then tested. For gas fields producing brine, the 18,300 ppm TDS (total dissolved solids) in the produced brine was reduced to 3060 ppm, an 83.3% rejection rate of 15,240 ppm salt rejection. For oilfield brine, while the TDS was reduced from 181,600 ppm to 148,900 ppm, an 18% rejection rate of 32,700 ppm reduction, the zeolite membrane was stable. Preliminary results show the dissolved organics, mainly hydrocarbons, did not affect the salt rejection. However, the rejection of organics was inconclusive at this point. Finally, the by-product of this project, the  $\alpha$ -alumina-supported Pt-Co/Na Y catalytic zeolite membrane was developed and demonstrated for overcoming the two-step limitation of nonoxidation methane ( $\text{CH}_4$ ) conversion to higher hydrocarbons ( $\text{C}_{2+}$ ) and hydrogen ( $\text{H}_2$ ). Detailed experiments to obtain quantitative results of  $\text{H}_2$  generation for various conditions are now being conducted. Technology transfer efforts included five manuscripts submitted to peer-reviewed journals and five conference presentations.

*Key Words: clay, supported membrane, sol-gel, mesoporous, reverse osmosis, desalination, MFI, zeolite membrane, ion separation, Pt-Co/NaY, catalytic membrane, nonoxidative, methane conversion, single step, hydrogen generation.*

## TABLE OF CONTENTS

DISCLAIMER .....	ii
ABSTRACT .....	iii
TABLE OF CONTENTS .....	iv
LIST OF TABLES .....	vi
LIST OF FIGURES .....	vii
ACKNOWLEDGEMENTS .....	ix
EXECUTIVE SUMMARY .....	1
INTRODUCTION .....	2
Project Objectives .....	2
TECHNOLOGY TRANSFER .....	3
CHAPTER 1: Preparation of $\alpha$ -Alumina-Supported Mesoporous Bentonite Membranes for Reverse	
Osmosis Desalination of Aqueous Solutions .....	4
1.1 Introduction .....	4
1.2 Experimental .....	6
1.2.1 Materials and Apparatus .....	6
1.2.2 Membrane Preparation and Characterization .....	9
1.2.3 RO Desalination Test .....	15
1.3 Discussion .....	17
1.4 Conclusions .....	20
1.5 References .....	21
CHAPTER 2: Desalination by Reverse Osmosis Using MFI Zeolite Membranes .....	23
2.1 Introduction .....	23
2.2 Experimental .....	24
2.2.1 Materials and Apparatus .....	24
2.2.2 Results and Discussions .....	26
2.3 Conclusions .....	29
2.4 References .....	30
CHAPTER 3: Reverse Osmosis of Ionic Aqueous Solutions on A MFI Zeolite Membrane;	
A Study of Salt Rejection Mechanisms .....	31
3.1 Introduction .....	31
3.2 Experimental .....	33
3.2.1 Materials and Chemicals .....	33

3.2.2	Membrane Synthesis.....	33
3.2.3	RO Experiment .....	34
3.3	Results.....	35
3.4	Discussion.....	36
3.5	Conclusions.....	40
3.6	References.....	41
CHAPTER 4: Zeolite Membrane Reverse Osmosis Desalination of Produced Water from		
	Oil and Gas Operations.....	44
4.1	Results of Desalination for Actual Produced Water .....	45
4.1.1	Desalination of Gasfield Produced Water from Farmington, New Mexico.....	46
4.1.2	Desalination of Oilfield Produced Water from Hobbs, New Mexico.....	48
CHAPTER 5: A Novel $\alpha$ -Alumina-Supported Pt-Co/NaY Catalytic Membrane to Overcome the Two-		
Step Limitation for the Nonoxidative Conversion of Methane.....		
5.1	Introduction.....	50
5.2	Experimental.....	52
5.2.1	Membrane Synthesis and Characterization.....	52
5.2.2	Membrane Reaction.....	53
5.3	Results.....	55
5.3.1	The Pt-Co/NaY Membrane.....	55
5.3.2	Nonoxidative CH <sub>4</sub> Conversion .....	58
5.4	Discussion.....	62
5.5	Conclusions.....	64
5.6	References.....	65

## LIST OF TABLES

Table 1-1. Chemical Compositions of the As-Received and Refined Clay Powders .....	8
Table 1-2. Effect of Suspension Composition on Membrane Formation by Dip-Coating .....	10
Table 1-3. Results of RO Desalination for a 0.1M NaCl Solution Using the Supported Clay Membranes .....	16
Table 1-4. Comparisons of Bentonite Clay Membranes for RO Desalination.....	20
Table 3-1. RO Separation Results for Single-Solute Solutions at 25°C .....	36
Table 3-2. Hydration Numbers (in the First Shell), Experimental ADHN, and Sizes of the Ions Involved in This Study <sup>[3-18]</sup> .....	38
Table 4-1. Composition of Gasfield Produced Water (pH = 7.25) (Farmington, New Mexico) .....	44
Table 4-2. Composition of Oilfield Produced Water (pH = 6.98) (Hobbs, New Mexico) .....	45
Table 4-3. Summary of RO Desalination Results on the MFI Membrane.....	46
Table 5-1. Chemical Composition of the Pt-Co/NaY Membrane Layer.....	54
Table 5-2. C2+ Formed during the Membrane Regeneration Process.....	54

## LIST OF FIGURES

Fig. 1-1. XRD patterns of the as-received and refined clay powders. ....	7
Fig. 1-2. Schematic diagram of the RO desalination system. ....	9
Fig. 1-3. Cross-section of a clay membrane prepared from a suspension containing 0.3 wt % bentonite and 0.1 wt % PVA and with a pH value of 7.5. ....	11
Fig. 1-4. SEM images of a clay membrane prepared from a suspension containing 0.7 wt % bentonite and 0.05 wt % PVA and with a pH value of 7.5. ....	12
Fig. 1-5. TEM image of an unsupported membrane prepared from the suspension used to synthesize the membrane in Fig. 1-4. ....	13
Fig. 1-6. XRD patterns of refined bentonite powders calcined at different temperatures. (d001, 45°C=10.32, d001,500°C=10.04A, d001, 600°C=10.02A, d001, 700°C=9.99A).....	14
Fig. 1-7. XRD patterns of the $\alpha$ -alumina support, clay powders, and the $\alpha$ -alumina-supported clay membrane calcined at 600°C. A – $\alpha$ -alumina substrate, B – refined bentonite powders fired at 600°C, C – $\alpha$ -alumina-supported bentonite membrane fired at 600°C. ....	15
Fig. 2-1. Schematic diagram of the RO system. ....	25
Fig. 2-2. Water flux and Na <sup>+</sup> rejection as functions of OR operation time for the 0.1M NaCl solution....	27
Fig. 2-3. Ion rejection as a function of operation time for the multicomponent feed solution containing 0.1M NaCl, 0.1M KCl, 0.1M NH <sub>4</sub> Cl, 0.1M CaCl <sub>2</sub> , and 0.1M MgCl <sub>2</sub> .. ....	28
Fig. 3-1. Schematic diagram of the RO system. ....	34
Fig. 3-2. Schematic illustration of the water and ion transport through a polycrystalline MFI membrane containing zeolitic pores and larger intercrystal pores.....	37
Fig. 3-3. Effect of cation valance on water and ion fluxes. ....	39
Fig. 3-4. Effect of cation size on water and ion fluxes. ....	40
Fig. 4-1. Cation rejection as a function of operation time for the gasfield produced water.....	46
Fig. 4-2. Anion rejection as a function of operation time for the gasfield produced water. ....	47
Fig. 4-3. Water flux as a function of operation time for the gasfield produced water. ....	47
Fig. 4-4. Cation rejection as a function of operation time for the oilfield produced water.....	48
Fig. 4-5. Anion rejection as a function of operation time for the oilfield produced water. ....	49
Fig. 4-6. Water flux as a function of operation time for the oilfield produced water. ....	49
Fig. 5-1. Schematic diagram of the membrane reactor system. ....	55

Fig. 5-2. XRD patterns of the substrate and supported NaY and Pt-Co/NaY membranes. (a) $\alpha$ -alumina substrate, (b) supported NaY membrane, (c) supported Pt-Co/NaY membrane.....	56
Fig. 5-3. Crystal morphology of the Pt-Co/NaY membrane surface. ....	56
Fig. 5-4. Cross-section SEM images of the membranes. (a) NaY membrane, (b) Pt-Co/NaY membrane.	57
Fig. 5-5. $C_2H_6$ production rate at the $CH_4$ feed side and $H_2$ sweep side as a function of operation time. Sweep flow: $12\text{ cm}^3$ (STP)/min ( $H_2:He = 1:5$ ).....	60
Fig. 5-6. $C_{2+}$ production rate on the $H_2$ sweep side as a function of operation time. Sweep flow: $14\text{ cm}^3$ (STP)/min ( $H_2/He = 1:2.5$ ).....	60
Fig. 5-7. MS spectrums of the permeate stream during membrane process at $250^\circ\text{C}$ . A – on Pt-Co/NaY membrane, B – on plain NaY membrane.....	61

## **ACKNOWLEDGEMENTS**

Many people have helped in this project who are not listed on the cover page: Liangxiong Li, Tina Nenoff, Xuehong Gu, and the student workers supporting us in the laboratories. Without all the generous help from everyone, this project would not be possible. Our thanks also go to the President's Office at the New Mexico Institute of Mining and Technology and to our supporters in New Mexico's oil and natural gas industry.

### **Students who assisted in this project**

#### **Postdoctoral**

Xuehong Gu

#### **Graduate students**

Liangxiong Li  
Jian Zhang  
Aniruddha Kulkarni

#### **Undergraduates**

Justin Monroe  
Vince McIntire  
Alexander Bourandas  
Marlene Axness  
Ashlee Ryan,  
Katsuya Sugimoto  
Amber Woodyatt

## EXECUTIVE SUMMARY

The original proposed Task II, Field Demonstration, of “Modified Reverse Osmosis System for Treatment of Produced Water,” DOE project No. DE-FC26-00BC15326, could not be delivered due to failure of salt rejection rates using compacted bentonite membranes. With the approval of DOE and additional financial support from New Mexico Tech President’s office, the project obtained a no-cost extension from the DOE, and the emphasis of the project was shifted to developing and testing supported thin clay membranes and exploring new technologies; in particular, reverse osmosis (RO) on molecular sieve zeolite membranes. Promising results were obtained, especially in the new technology of RO on thin zeolite membranes, which are documented in this report:

1. *Supported Bentonite Membranes:* Mesoporous bentonite clay membranes approximately 2–5  $\mu\text{m}$  thick were prepared on porous  $\alpha$ -alumina substrates by a sol-gel method. The membranes were tested for reverse osmosis (RO) separation of a 0.1 M NaCl solution. The  $\text{Na}^+$  rejection rate was comparable to compacted membranes tested in the first part of this project. However, their total permeability to water was significantly higher than that of the compacted thick membranes. Unfortunately, the bentonite membranes absorbed water molecules in the interlayer spaces that prop the clay sheets apart. Apparently, a better membrane must be found to provide steady salt rejection during operations. On the other hand, the supported bentonite membranes are being used to test gas/gas separations in our laboratories and may prove useful for this purpose.
2. *Synthetic Zeolite Membranes:* An  $\alpha$ -alumina-supported MFI-type zeolite membrane synthesized by in-situ crystallization was fabricated and tested. Various ion rejection rates were obtained. Unlike the bentonite clay membranes, the zeolite membranes maintained stability and high salt rejection rate even for a highly saline solution. Actual produced brines from gas and oil fields were tested next. For gas field-produced brines, the 18,300 ppm TDS (total dissolved solids) in the produced brine was reduced to 3060 ppm, an 83.3% rejection rate of 15,240 ppm salt rejection by a single cycle operation. For oilfield brine, while the TDS was reduced from 181,600 ppm to 148,900 ppm, an 18% rejection rate of 32,700 ppm reduction, the zeolite membrane was stable. Preliminary results show the dissolved organics, mainly hydrocarbons, did not affect salt rejection. However, rejection of organics was inconclusive at that point. The decline of ion rejection at extremely high concentration was attributed to diminishing separation through the defective intercrystal pores. Improvement of the zeolite membranes for oil/gas fields produced water is being conducted.
3. *Methane Conversion:* A new type of  $\alpha$ -alumina-supported Pt-Co/Na Y catalytic zeolite membrane was developed and demonstrated for overcoming the two-step limitation of nonoxidation methane ( $\text{CH}_4$ ) conversion to higher hydrocarbons ( $\text{C}_{2+}$ ) and hydrogen ( $\text{H}_2$ ).

Current produced water treatments mainly evolved from “sea water” technology, and can only deal with low saline brine. Moreover, the removal of organics is the key—an expensive but necessary step to prolong the life of the membranes used in a reverse osmosis process. The zeolite membranes developed in this study are insensitive to organics and can achieve high salt rejection in high saline produced brine. Furthermore, preliminary data showed their potential to remove organics and salt simultaneously by RO because of the unique mechanisms of size exclusion and competitive diffusion. More detailed laboratory work and economic evaluations must be conducted to test the feasibility of using zeolite membranes for produced brine treatments.

The supported bentonite clay membranes are currently being investigated to separate  $\text{CO}_2$  from flue gas ( $\text{N}_2 + \text{CO}_2$ ) at high temperatures for  $\text{CO}_2$  sequestration. The study of the byproduct of this project, the use of catalytic zeolite to generate  $\text{H}_2$  from  $\text{CH}_4$ , will be continued in our laboratories.

## **INTRODUCTION**

In the United States, more than 20 billion barrels of water are produced each year during oilfield operations. Disposal of produced water can be expensive. For example, produced water in the San Juan Basin of New Mexico and Colorado is currently disposed of by deep-well injection at a cost of approximately \$1.75 per bbl. In other areas the cost of water disposal is typically between \$0.25 and \$0.50 per barrel for pipeline transport and \$1.50 per barrel for trucked water.

In many parts of the country, deep injection wells, or use of produced water for waterflood operations, may not be available disposal options. The EPA commonly will not allow surface disposal of produced waters because of the high content of dissolved solids. Therefore, in many areas, produced water will need to be treated prior to disposal so that it can meet EPA standards for various uses such as surface disposal, fresh water aquifer recharge, drinking water, irrigation, or release to streams.

## **PROJECT OBJECTIVES**

Work this year focused on testing clays for use as reverse osmosis membranes to remove dissolved solids from oilfield produced waters. Geologists have known for many years that clays exhibit osmotic or membrane properties.

Current produced water treatments evolved mainly from “sea water” technology, and can only deal with low saline brines. Moreover, the removal of organics is the key—an expensive but necessary step to prolong the life of the membranes used in a reverse osmosis process. The Zeolite membranes developed in this study are insensitive to organics and can achieve high salt rejection in high saline produced brines. Furthermore, preliminary data showed the possibility of removing organics and salt simultaneously by RO on zeolite membranes because of the unique mechanisms of size exclusion and competitive diffusion. More detailed laboratory work and economic evaluations must be conducted to test the feasibility of using zeolite membranes for produced brine treatments.

## TECHNOLOGY TRANSFER

### PEER-REVIEWED PUBLICATIONS

#### JOURNALS

1. L. Li, J. Dong, R. Lee, "Alpha-Alumina Supported Microporous Bentonite Clay Membranes for Gas and Liquid Separation," *J. Colloid. Interf. Sci.*, (2003), in press.
2. X. Gu, J. Dong, T.M. Nenoff, L. Li, R. Lee, "A Novel  $\alpha$ -Alumina-Supported Pt-Co/NaY Catalytic Membrane to Overcome the Two-Step Limitation for the Nonoxidative Conversion of Methane," *J. Catal.*, (2003) (submitted).
3. L. Li, J. Dong, T.M. Nenoff, R. Lee, "MFI Type Zeolite Membranes for Reverse Osmosis Desalination of Aqueous Solutions," *J. Membr. Sci.* (2003) (submitted).
4. L. Li, J. Dong, T.M. Nenoff, R. Lee, "Reverse Osmosis of Ionic Aqueous Solutions on A MFI Zeolite Membrane," *Desalination*, (2003), (submitted).
5. L. Li, J. Dong, T.M. Nenoff, R. Lee, "Synthesis of Microporous Alumina-Pillared K-Bentonite Membranes for  $N_2/CO_2$  Separation. Micropor." *Mesopor Mat.*, (in preparation).

#### CONFERENCES

1. L. Li, J. Dong, R. Lee, "Preparation of  $\alpha$ -Alumina-Supported Mesoporous Bentonite Membranes for Reverse Osmosis Desalination of Aqueous Solutions," AIChE Annual meeting, San Francisco, CA, Nov. 16 - 21, 2003.
2. L. Li, J. Dong, T. M. Nenoff, R. Lee, "Desalination by Reverse Osmosis Using MFI Zeolite Membranes," AIChE Annual meeting, San Francisco, CA, Nov. 16 - 21, 2003.
3. GTI conference paper. L. Li, J. Dong, T.M. Nenoff, R. Lee. "Ion Transport through MFI Zeolite Membrane," Natural Gas Technologies II: Ingenuity & Innovation. Phoenix, February 8-11, 2004.

## CHAPTER 1

### Preparation of $\alpha$ -Alumina-Supported Mesoporous Bentonite Membranes for Reverse Osmosis Desalination of Aqueous Solutions

In this study, mesoporous bentonite clay membranes approximately  $2\mu\text{m}$  thick were prepared on porous  $\alpha$ -alumina substrates by a sol-gel method. Nanosized clay particles were obtained from commercial Na-bentonite powders (Wyoming) by a process of sedimentation, washing, and freeze-drying. X-ray diffraction (XRD), scanning electron microscopy (SEM), transmission electron microscopy (TEM), and nitrogen adsorption-desorptions (BET) were employed for membrane characterizations. It was found that the content of solid, concentration of polymer binder, and pH value of the clay colloidal suspension had critical influences on membrane formation during the dip-coating process. The membranes were tested for reverse osmosis (RO) separation of a 0.1M NaCl solution. Both water permeability and  $\text{Na}^+$  rejection rate of the supported membranes were comparable to those of the compacted thick membranes reported in the literature. However, due to the drastically reduced membrane thickness, water permeance and flux of the supported membranes were significantly higher than those of the compacted thick membranes. It was also observed that the calcination temperature played a critical role in determining structural stability in water and desalination performance of the clay membrane.

#### 1.1 Introduction

Naturally occurring clays are crystalline materials with a layered structure composed of octahedral flat sheets. The major constituents of clays are  $\text{Al}_2\text{O}_3$  and  $\text{SiO}_2$  with a variety of oxides that make clays of different types. The thickness of a single sheet is around  $9.5\text{--}10\text{\AA}$  for smectite clays.<sup>[1-1]</sup> The clay surface is negatively charged due to ion substitutions. Cations, often  $\text{Na}^+$  or  $\text{Ca}^{2+}$ , exist in the interlayer space as charge compensators. When contacting liquid water, charged double layers form at the clay surfaces.

In compact clay structures, the charged double layers can overlap in the mesoporous or microporous system. The overlapping double layers can reject hydrated ions while allowing water and electrically neutral species to enter the pores freely. <sup>[1-2,1-3]</sup> Therefore, naturally occurring clay barriers can restrict ion transport during permeation of aqueous solutions. Over the past three decades, many efforts have been made to understand ion and water transport behavior in compact clay barriers in the interests of modeling the groundwater flow and evolution of groundwater salinity and in order to develop environment-protective liners for landfill and brine basins. <sup>[1-4]</sup>

More recently, compacted clay membranes were studied as potential reverse osmosis (RO) membranes for removal of ions from water. <sup>[1-5-1-7]</sup> The compacted clay membranes were formed from slurry sedimentation, compacted in molds under high hydraulic pressures, and then tightly sandwiched between strong and rigid supports, e.g. thick, porous stainless steel plates, to prevent fracturing and deformation of the membranes during transfer and water permeation. The membranes are usually composed of refined submicron or nanosized clay particles, which form small interparticle pores to allow formation of overlapping double layers. Such compacted clay membranes have shown good ion rejection but low flux compared to polymeric RO membranes. <sup>[1-2,1-8]</sup>

Clay membranes, due to their chemical and thermal stabilities, may be potentially useful for separations that cannot be handled by polymeric RO membranes; for instance, desalination of water containing organic solvents and separation of radioactive ions from low-level wastewater. However, the compacted clay membranes are impractical due to their extreme brittleness and thickness (hence their high transport resistance). To make the clay membranes practical, supported thin membranes must be developed.

Only a few reports regarding supported clay membranes are found in the literature, all focusing on pillared clay (PILC) for gas separation. Vercauteren and coworkers <sup>[1-9,1-10]</sup> synthesized  $\text{Al}_2\text{O}_3$ -pillared montmorillonite membranes on mesoporous  $\gamma$ -alumina membranes. The thin PILC membranes (thickness < 0.5  $\mu\text{m}$ ) were made by dip-coating with a 0.1 wt% suspension of plain clay particles followed

by drying, pillaring and firing. Although the clay particle size was 0.2–0.5 $\mu\text{m}$  by light scattering measurement, the resultant membranes had a microporous structure with a mean pore size (interlayer space) of 0.8 nm and surface area of 266–314  $\text{m}^2 \text{g}^{-1}$ . The main reasons causing the microporous structure were suggested to be (i) effective pillaring (ii) small primary layer plates ( $\sim 0.1 \mu\text{m}$ ), and (iii) ordered layers of clay plate that minimized the interparticle pores.<sup>[1-11]</sup> The membranes exhibited Knudsen diffusion behavior for  $\text{H}_2/\text{N}_2$  with a selectivity of 3.6 and  $\text{N}_2$  permeance of  $2 \times 10^{-8} \text{ mol m}^{-2} \text{ s}^{-1} \text{ Pa}^{-1}$  at 175°C. Hu et al. <sup>[1-12]</sup> prepared porous glass-supported  $\text{Al}_2\text{O}_3$ -PILC membranes by deposition of uncalcined PILC from suspensions. After firing, the membrane was treated by impregnation and carbonization of polyvinyl alcohol to reduce the interparticle pores. Good separation was obtained for  $\text{N}_2$ /aromatic vapor mixtures by a diffusion mechanism.

This study aims to synthesize mesoporous bentonite clay thin membranes on the practical macroporous  $\alpha$ -alumina substrates using a sol-gel method. The synthesized membranes will be characterized by X-ray diffraction and electron microscopic techniques and tested for RO desalination of NaCl solutions.

## 1.2 Experimental

### 1.2.1 Materials and Apparatus

Homemade  $\alpha$ -alumina discs 28 mm in diameter and 2 mm thick were used as substrates. The substrates had a mean pore size of about 0.15 $\mu\text{m}$  and porosity about 40%. The  $\alpha$ -alumina powders were provided by Alcoa (mean particle size 0.44 $\mu\text{m}$ ). The coating side of the alumina disc was polished by #600 sandpaper and washed by deionized (DI) water. Polyvinyl alcohol (PVA, Mw = 31,000–50,000, 98–99%, Aldrich) was used as binder to prevent crack formation during drying and the early stage of firing. Other chemicals used in this study include NaCl (>99.5%, Alfa Aesar), nitric acid (0.998N, Aldrich), and nitrogen (>99.9%, TriGas) which were all used as received.

Pure bentonite nano-powders were obtained from the commercial Wyoming Na-bentonite particles (WYO-Ben®, Wyo-Ben Hydrogel) by a multiple-step process including separation, washing, and drying. In the first step, nanosized bentonite particles (mean particle size <50 nm) were separated from the commercial powders by a sedimentation technique. In the second step, the collected bentonite clay slurry was washed with DI water until it was free of dissolvable salts (confirmed by conductivity measurements for the supernate from the centrifuge). In the third step, the slurry of pure bentonite was freeze-dried in a Labconco benchtop freeze dryer (Model 4.5). The bentonite dry powders were redispersed before use. Figure 1-1 shows the X-ray diffraction (XRD) patterns of the as-received clay particles and the refined bentonite powders. A comparison of the XRD patterns showed that quartz and other heavy mineral components were removed by sedimentation and washing. The chemical compositions of the clay powders before and after refining were measured by X-ray fluorescence (XRF) (Phillips PW2400 wavelength dispersive X-ray spectrometer with Rh and window tube controlled by X40 software) as shown in Table 1-1.

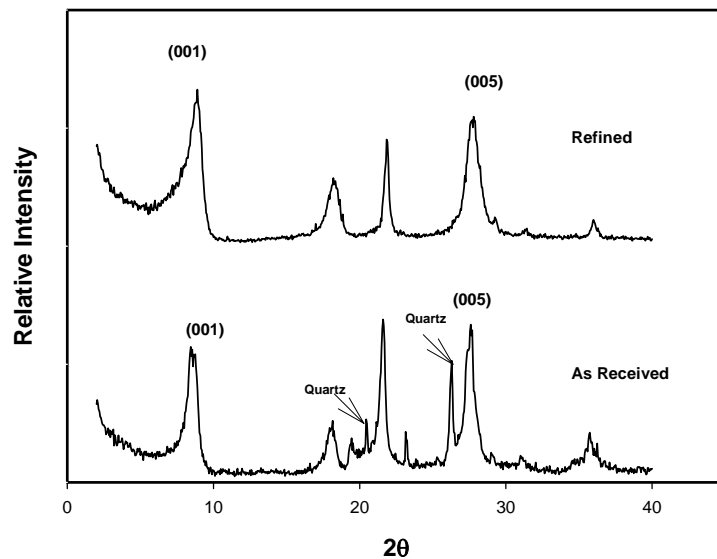


**Fig. 1-1.** XRD patterns of the as-received and refined clay powders.

**Table 1-1.** Chemical Compositions of the As-Received and Refined Clay Powders

Component	As-received	Refined
SiO <sub>2</sub>	68.1	65.4
TiO <sub>2</sub>	0.149	0.111
Al <sub>2</sub> O <sub>3</sub>	14.6	14.2
Fe <sub>2</sub> O <sub>3</sub> -T	3.25	3.01
MnO	0.020	Undetectable
MgO	1.67	1.80
CaO	1.17	0.696
Na <sub>2</sub> O	2.03	3.08
K <sub>2</sub> O	0.447	0.101
P <sub>2</sub> O <sub>5</sub>	0.060	0.020
LOI	8.54	11.6
Total	100	100
Ba	291	73

Note: Fe<sub>2</sub>O<sub>3</sub>-T is total iron expressed as Fe<sub>2</sub>O<sub>3</sub>; LOI is the loss on ignition; all values are in weight percent except for Ba, which is in parts per million.

X-ray diffraction (XRD, Rigaku® Geigerflex) was used to analyze the crystal structure of the clay powders and membranes. A scanning electron microscopy (SEM, JEOL 5800LV) and a transmission electron microscopy (TEM, JEOL 2010) were used to estimate the thickness and observe the morphology and microstructure of the membranes. The membranes were tested for RO desalination of a 0.1M NaCl solution.

The RO desalination system is shown schematically in Fig. 1-2. The clay membrane was mounted in a stainless steel cell with the membrane side facing the feed stream. The feed pressure was maintained by a nitrogen cylinder and the feed flow rate was controlled by a needle valve located at the exit of the feed chamber. The liquid permeate was received by a sample bottle at atmospheric pressure. The sample bottle was connected to the gas phase of a water bottle to prevent evaporation of

the collected sample.  $\text{Na}^+$  concentration of the solutions was analyzed by a dual-column ion chromatograph (IC, DX120, Dionex) with an IC workstation.

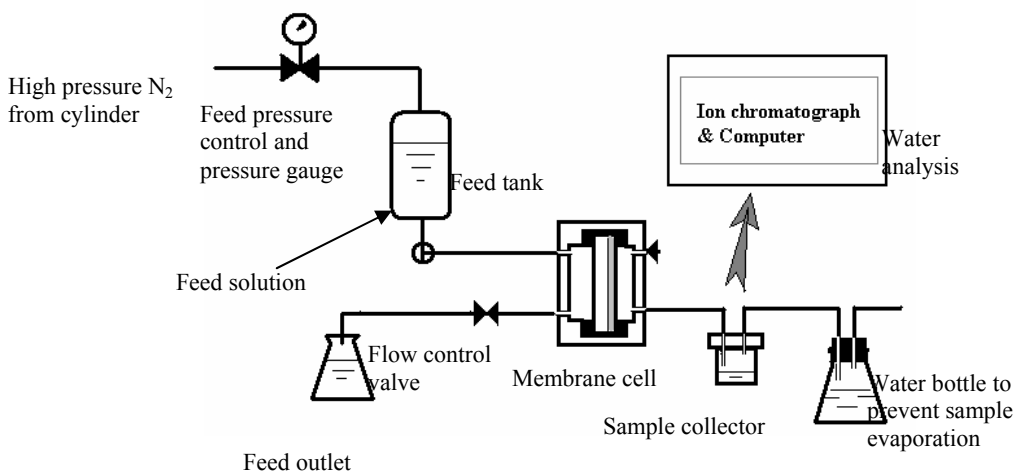


**Fig. 1-2.** Schematic diagram of the RO desalination system.

### 1.2.2 Membrane Preparation and Characterization

The  $\alpha$ -alumina-supported bentonite thin membranes were prepared by the following procedure: The refined bentonite powders were redispersed into DI water (1.5wt % of bentonite) by two hours of rigorous agitation and thirty minutes of an ultrasonic bath. The resulting clay suspension was very stable. No solid sedimentation was observed after being placed statically for one week. The 0.5 wt % PVA solution was prepared by dissolving 0.5g PVA solid into 99.5g DI water and filtering through a Whatman® #2 filter paper. The bentonite suspension was mixed with the PVA solution with a controlled ratio under stirring. The pH value of the suspension was controlled by adding 0.2 N  $\text{HNO}_3$  or 0.1N  $\text{NaOH}$  solutions. The resulting bentonite suspension was dispersed again in an ultrasonic bath for fifteen minutes followed by twenty minutes of rigorous stirring before use.

The pH value, solid content, and (PVA) binder concentration of the synthesis suspension were varied to identify the appropriate conditions for membrane formation. The membrane was coated by dipping the polished side of the substrate into the synthesis suspension for five seconds. The dip-coated

membranes were dried at 40°C in air with controlled relative humidity of about 60% for two days. After the drying process, the membranes were calcined in air at different temperatures to study the effect of calcination temperature on the membrane properties. All the firing programs used a heating rate of 0.5°C/min and a cooling rate of 1°C/min. In some cases, the dip-coating process was repeated once or more after calcination. Results of membrane coating with various suspension compositions are given in Table 1-2.

**Table 1-2.** Effect of Suspension Composition on Membrane Formation by Dip-Coating

Solid, wt%	PVA, wt%	pH	Membrane formation
>0.9	0.05 – 0.2	3.0 – 9.5	Thick and uneven layers; peeled off after drying
0.5 – 0.8	0.05 – 0.15	<5.0	Thick and uneven layers; cracked after drying
0.5 – 0.8	>0.1	4.0 – 9.5	Thick and uneven layers; peeled off after drying
0.5 – 0.8	~ 0.05	7 – 9	Uniform and crack-free by single coating
<0.35	0.01 – 0.05	7 – 9	Uniform and crack-free; particles penetrated into substrate

Bentonite suspensions of low pH values, high solid contents, and high PVA concentrations resulted in thick and uneven layers during the first dip-coating due to flocculation in the suspension and rapid and excessive gelation at the substrate surface. Contrarily, the nanoscale bentonite particles penetrated deeply into the substrate pores when the solid content was less than 0.35 wt %, because the clay particles failed to gelate and bridge over the substrate pore openings when the solid content was too low. Figure 1-3 is the SEM image of a typical clay membrane obtained by coating with a suspension containing 0.3 wt % bentonite and calcined at 450°C in air for three hours. The dip-coating process was repeated twice. Clay particle penetration into the alumina substrate was clearly observed.

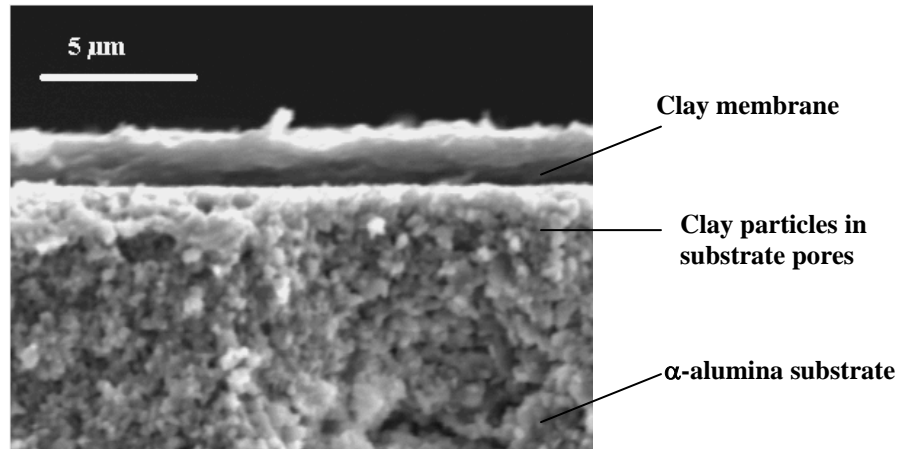
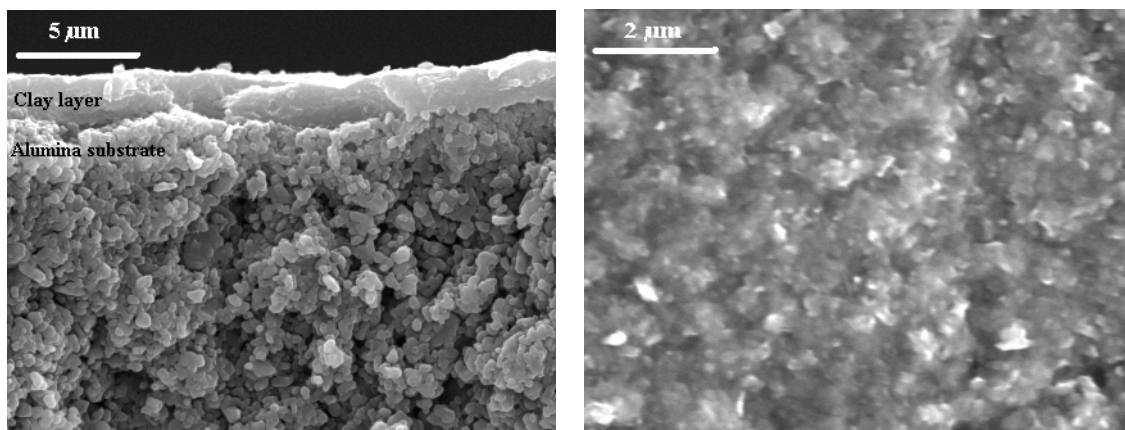


**Fig. 1-3.** Cross-section of a clay membrane prepared from a suspension containing 0.3 wt % bentonite and 0.1 wt % PVA and with a pH value of 7.5.

Defect-free membranes were obtained by single coating using a suspension containing 0.7 wt % bentonite, and 0.05 wt % PVA, with pH of 7.5. After the first coating, the fired clay membrane was no longer able to ingest liquid with a rate appropriate for the dip-coating process. A thin liquid film remained on the membrane surface after contacting the suspension for one second, suggesting that the membrane had a microporous structure and/or very low porosity. SEM observations showed that the membrane thickness did not change significantly with the number of dip coatings. Membranes prepared by single coating, double coating, and triple coating were found to have similar thicknesses of about  $2\mu\text{m}$ .

Figure 1-4 shows the SEM images of a clay membrane obtained by single-coating with a suspension containing 0.7 wt% of bentonite. The membrane was dried and then fired at  $500^{\circ}\text{C}$  for three hours in air.



(a) cross-section

(b) surface

**Fig. 1-4.** SEM images of a clay membrane prepared from a suspension containing 0.7 wt % bentonite and 0.05 wt % PVA and with a pH value of 7.5.

The cross-sectional SEM picture indicates a uniform clay membrane formed on the alumina substrate without particle penetration. Cracks were not found in the area of the specimen by random searching.

Figure 1-5 is a TEM image showing the microstructure of an unsupported membrane obtained from the suspension used for dip coating the membrane shown in Fig. 1-4 and fired at identical conditions. The TEM image showed the majority of the particles were smaller than 50 nm of diameter.

Three samples of unsupported membranes were prepared by naturally drying the remaining suspensions of membrane coating and calcining them together with the supported membranes. BET tests of the three unsupported membrane samples revealed a mesoporous structure. The average BET surface area of the three samples was about  $58 \text{ m}^2 \text{ g}^{-1}$  with pore volume of  $0.075 \text{ cm}^3 \text{ g}^{-1}$  and average pore size of 5.2 nm. Microporous area and micropore volume were negligible because, without solid pillars, the interlayer spaces closed after being dried as confirmed by the measurement of  $d_{001}$  values using XRD.

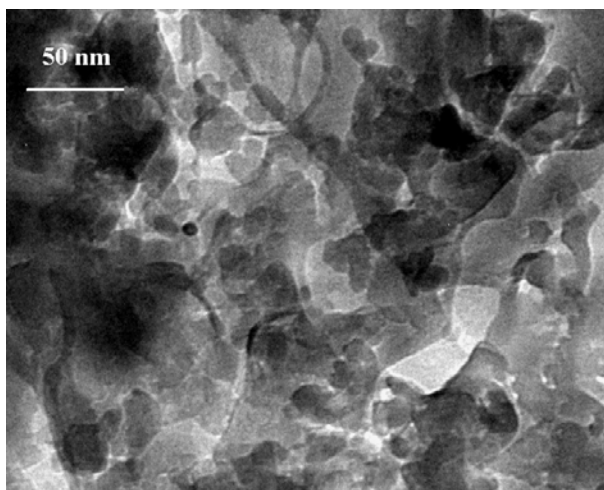


**Fig. 1-5.** TEM image of an unsupported membrane prepared from the suspension used to synthesize the membrane in Fig. 1-4.

The refined clay powders were calcined in air, and then tested by ex-situ XRD to examine the thermal stability of the crystallographic structure. Figure 1-6 shows the XRD patterns of the clay powders calcined at different temperatures for three hours. The crystal structure was stable after being fired at 700°C. However, the  $d_{001}$  value was found to decrease from 10.32Å to 9.99Å when the heat treatment temperature increased from 45 to 700°C. The  $d_{001}$  is the distance between the upper surfaces of two neighboring layers, namely the sum of the single layer thickness and the interlayer space. The  $d_{001}$  values around 10Å indicate closure of the interlayer space after being dried at 45°C for 48 hours, because the thickness of the octahedral clay plates is about 9.6Å<sup>[1-10, 1-13]</sup>.

The XRD pattern of the alumina-supported clay membrane (shown in Fig. 1-7) is clearly a combination of the XRD patterns of  $\alpha$ -alumina substrate and clay powders. The low relative intensities of the clay peaks, compared to the strong peaks from the  $\alpha$ -alumina substrate, verify a very thin clay membrane.

The porosity and the packing style of the dried clay depend on the preparation conditions.<sup>[1-10]</sup> Natural sedimentation and slow drying processes result in oriented sheet stacks that possess minimized inter-particle mesopores while freeze-drying or fast deposition leads to a randomly oriented “card house”

structure that consists of a high degree of mesoporous volume. <sup>[1-11]</sup> The XRD patterns of the dip-coated membranes had identical relative intensities compared to those of the freeze-dried powders (Fig. 1-7), indicating the membrane was composed of randomly packed clay particles.

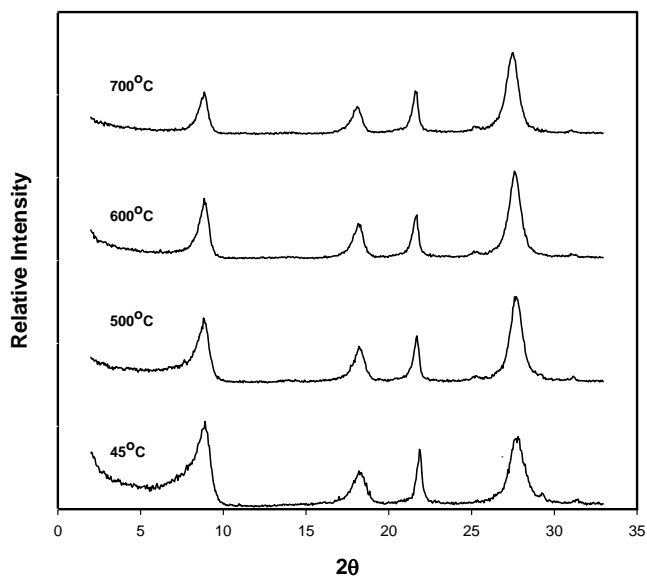


**Fig. 1-6.** XRD patterns of refined bentonite powders calcined at different temperatures. ( $d_{001, 45^{\circ}\text{C}}=10.32$ ,  $d_{001, 500^{\circ}\text{C}}=10.04\text{\AA}$ ,  $d_{001, 600^{\circ}\text{C}}=10.02\text{\AA}$ ,  $d_{001, 700^{\circ}\text{C}}=9.99\text{\AA}$ )

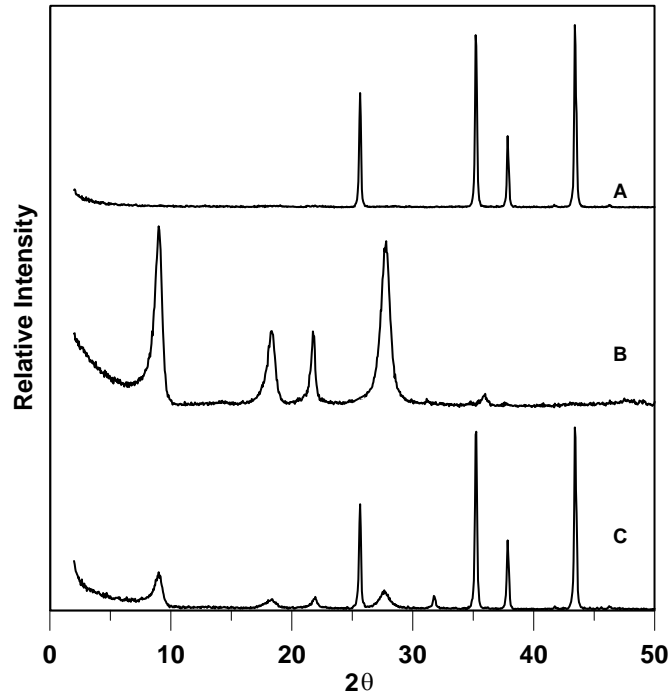


**Fig. 1-7.** XRD patterns of the  $\alpha$ -alumina support, clay powders, and the  $\alpha$ -alumina-supported clay membrane calcined at 600°C. **A** –  $\alpha$ -alumina substrate, **B** – refined bentonite powders fired at 600°C, **C** –  $\alpha$ -alumina-supported bentonite membrane fired at 600°C.

### 1.2.3 RO Desalination Test

Clay membranes were prepared by a single dip-coating process using the optimized suspension (0.7 wt % bentonite and 0.05 wt % PVA, with pH = 7.5). Different firing temperatures were used to study the effect of heat treatment on the membrane performance in RO desalination of a 0.1M NaCl solution. The results are given in Table 1-3. Ion rejection,  $r$ , is given by equation (1-1),

$$r = \frac{(C_s)_{feed} - (C_s)_{perm}}{(C_s)_{feed}} \times 100\% \quad (1-1)$$

where  $(C_s)_{feed}$  and  $(C_s)_{perm}$  are concentrations of the feed and permeate solutions, respectively.

**Table 1-3.** Results of RO Desalination for a 0.1M NaCl Solution Using the Supported Clay Membranes

Calcination conditions	Thickness, $\mu\text{m}$	$p_f^*$ , MPa	Flux, $\text{mol}\cdot\text{m}^{-2}\cdot\text{h}^{-1}$	$r$ , %
450°C for 3h	~2.0	0.41	34.11	4.5
500°C for 3h	~2.0	0.82	8.33	44.5
600°C for 3h	~2.0	No flux under feed pressure of up to 1.03 MPa		
700°C for 3h	~2.0	No flux under feed pressure of up to 1.03 MPa		

\* $p_f$  – feed side pressure (gauge).

The membrane calcined at 500°C exhibited a  $\text{Na}^+$  rejection of 44.5% and a water flux of  $8.33 \text{ mol}\cdot\text{m}^{-2}\cdot\text{h}^{-1}$  in the first five hours. The water flux decreased with time and stabilized at  $5.5 \text{ mol}\cdot\text{m}^{-2}\cdot\text{h}^{-1}$  in 50 h while the rejection was essentially unchanged. The membrane remained solid without peeling off and observable swelling after about 60 h of operation. The membrane, however, became soft due to swelling after being immersed in the NaCl solution for more than 72 h but still did not peel off. The swollen membrane remained its integrity and could be reconsolidated by drying and calcination.

The membrane calcined at 450°C had an extraordinarily high water flux of  $34.11 \text{ mol}\cdot\text{m}^{-2}\cdot\text{h}^{-1}$  at a low applied pressure of 0.41 MPa. However, the rejection was extremely low, only 4.5%. The membrane was found to swell and peel off from the substrate after 30 hours of permeation testing.

For the membranes fired at 600°C and 700°C, no water permeation was observed in 30 h under an applied pressure of 1.03MPa, which is the maximum pressure that the alumina substrate could withstand. The membranes remained solid without swelling after being immersed in the NaCl solution for three days.

### 1.3 Discussion

In the non-pillared clay structure, water molecules are adsorbed both physically (free molecules) and chemically (hydrates) in the interlayer spaces that prop the clay sheets apart.<sup>[1-14]</sup> During the thermal consolidation of the membranes, the degree of dehydration increases with temperature and treating time. At low firing temperatures, e.g. 450°C in this study, dehydration may be incomplete and reversible. When the calcined membrane contacts water, rehydration occurs that causes swelling and deformation of the clay film.<sup>[1-15]</sup> Swelling and deforming of the clay particles may destroy the integrity of the clay membrane that results in high water flux and low ion rejection.

It appears that there is a threshold firing temperature, e.g. 500–600°C in this study, above which dehydration becomes irreversible. This irreversibility of dehydration is likely caused by two reasons: the first is the decrease in interlayer distance and reduction of active porosity that prevent water molecules from reentering the interlayer space<sup>[1-11, 1-16]</sup>; and the second is the decrease in hydrophilicity of the clay surface with increasing the firing temperature.<sup>[1-17]</sup> Therefore, the effective pathway for water permeation in the membrane is the intercrystal mesopores rather than the interlay spaces.

Interlayer spacing in the clay crystals is affected by the supporting species such as adsorbed water molecules, ions, and implanted pillars. Although sintering effects are unlikely to occur in the clay films even at the highest firing temperature (700°C) used in this work, significant reduction of the active intercrystal pore volume may be caused by decreases in interlayer spacing as dehydration deepens.<sup>[1-16, 1-18]</sup> The reduction of active pore volume might have caused the diminishing water permeability of the membranes fired at 600°C and 700°C. Moreover, the hydrophobicity of the clay surface may increase with firing temperature that increases the resistance of water transport in its mesoporous system.

In Table 1-4, RO desalination results of the supported membrane calcined at 500°C are compared with those of compacted membranes reported in the literatures. The stabilized water flux of the supported

membrane is used in the comparison. The flux ( $F$ ), permeance ( $P_a$ ), and permeability ( $P_b$ ) are defined by the following equations:

$$P_b = P_a \delta \quad (1-2)$$

$$P_a = \frac{F}{\Delta P} = \frac{F}{p_f - p_p - \Delta\pi} \quad (1-3)$$

$$F = \frac{Q_w}{A_m \cdot t} \quad (1-4)$$

$$\Delta\pi = \left[ \left( \frac{C_s}{100 - C_s} \right)_{perm} - \left( \frac{C_s}{100 - C_s} \right)_{feed} \right] \frac{RT}{M_w} \quad (1-5)$$

where  $\delta$  is the membrane thickness;  $\Delta\pi$  is the difference between osmosis pressures of the feed and permeate solutions;  $p_f$  and  $p_p$  are pressures at the feed and permeate side, respectively;  $Q_w$  is the quantity of water collected in a time period of  $t$ ;  $A_m$  is the effective membrane area;  $T$  is the temperature;  $R$  is the gas constant; and  $M_w$  is the molecular weight of the cation.

Permeability is a membrane property that is independent of membrane thickness but mainly dependent of the microstructure and surface properties. The differences among the water permeability values of all the membranes, compacted and supported, are within a close range, indicating the supported and the compacted membranes had a similar microstructure and surface hydrophilicity. The water permeability of the supported membrane was lower than that of the compacted membranes, most likely due to its reduced pore volume caused by firing compared to the unfired compacted membranes.

The pressure-independent permeance ( $P_a$ ) can be thought of as an index measuring the ease or difficulty for a fluid to permeate through the membrane. Water permeance through the supported membrane was significantly higher than it was for the compacted membranes. The extraordinarily high

water permeance on the supported membrane was due primarily to the thinness of the membrane, which resulted in significantly lowered resistance for mass transport.

Ion rejection depends not only on the microstructure and chemistry of the clay membranes but also on the concentration and pH of the feed solution. The result of this work is compared with our previous data on a compacted membrane made of the same clay powder.<sup>[1-7]</sup> The rejection of the supported membrane is lower than that of the compacted membrane. The possible reasons include: (i) The supported membrane prepared by a single coating process likely contained some non-selective microdefects, and (ii) The firing process might have reduced the separative pore volume.

Despite the relatively low rejection rates, the supported thin membranes are superior to the compacted membranes because of the dramatically lowered operation pressure and enhanced water permeance.

**Table 1-4.** Comparisons of Bentonite Clay Membranes for RO Desalination

Mem*	Solution	$\delta$ $\mu\text{m}$	$P_f$ MPa	Flux $\text{mol}\cdot\text{m}^{-2}\cdot\text{h}^{-1}$	Permeance $\text{mol}\cdot\text{m}^{-2}\cdot\text{kPa}^{-1}\cdot\text{h}^{-1}$	Permeability $\text{mol}\cdot\text{m}^{-1}\cdot\text{kPa}^{-1}\cdot\text{h}^{-1}$	$r$ , %	Ref.
CP	0.60M NaCl	2200	27.4	0.088	$3.21\times 10^{-6}$	$7.06\times 10^{-8}$	60.0	( 2 )
CP	0.8M NaCl+0.15M CaCl <sub>2</sub>	5000	13.9	0.452	$3.25\times 10^{-5}$	$1.62\times 10^{-7}$	60.0	( 5 )
CP	5.04M NaCl + 0.45M CaCl <sub>2</sub>	16,000	13.8	0.275	$1.99\times 10^{-5}$	$3.19\times 10^{-7}$	25.0	( 6 )
CP	0.10M NaCl	60	5.2	7.22	$1.38\times 10^{-3}$	$8.33\times 10^{-8}$	62.9	( 7 )
SP	0.10M NaCl	2	0.82	5.5	$6.71\times 10^{-3}$	$1.34\times 10^{-8}$	44.5	This study

\* CP – compacted; SP – supported.

## 1.4 Conclusions

In this study, mesoporous bentonite clay membranes (about 2  $\mu\text{m}$  thick) were synthesized on porous  $\alpha$ -alumina substrates by a sol-gel method using refined clay nano-powders. The supported membranes exhibited reasonably good ion rejection in RO separation of a 0.1M NaCl solution. The 2  $\mu\text{m}$ -thick supported membrane achieved water permeance that was four times higher while the operation pressure was five times lower than that obtained on the thinnest compacted membrane (thickness=60 $\mu\text{m}$ ) reported in the literature. The supported clay membranes are potentially useful in water treatment processes where polymeric RO membranes are not applicable, such as ion removal from wastewater containing organic solvents and low-level radioactive wastewater. However, further investigations are required to understand the effects of synthesis conditions on the microstructure and chemical stabilities of the membrane materials as well as their effects on the membrane performance. The membranes may also be further modified into microporous PILC membranes by a swelling and pillaring process for applications in gas separation.

## 1.5 References

- [1-1] Reinholdt, M., et al.: "Fluorine Synthesis of Montmorillonite Containing Mg and Zn and Characterization by XRD, Thermal Analysis, MAS NMR, and EXAF Spectroscopy," *Euro. J. Inorganic Chem.*, (2001), 2831.
- [1-2] Yousif, K. K., and Frederick, A. F. B.: "Simultaneous Flow of Water and Solutes through Geological Membranes-I Experimental Investigation," *Geochimica et Cosmochimica Acta*, 37 (1973) 2577.
- [1-3] Ishiguro, M., Matsuura, T. and Detellier, C.: "Reverse Osmosis Separation for a Montmorillonite Membrane," *J. of Membrane Sci.* 107 (1995) 87.
- [1-4] Wijeyesekera, D. C., O'Connor, K., and Salmon, D. E. "Design and Performance of a Compacted Clay Barrier through a Landfill," *Engineering Geology*, 60 (2001) 295.
- [1-5] William, M. B., and Donald, L. G. "Studies of Smectite Membrane Behavior: Importance of Layer Thickness and Fabric in Experiments at 20°C," *Geochimica et Cosmochimica Acta*, 48 (1984) 1769.
- [1-6] Paul, R. H., and Donald, L. G. "Studies of Smectite Membrane Behavior: Temperature Dependence, 20-80°C," *Geochimica et Cosmochimica Acta.* 50 (1985) 115.
- [1-7] Li, L. X., Whitworth, T. M., and Lee, R. "Construction of an Ultra-Thin, Compacted Clay Membrane for Use in Reverse Osmosis," *Applied Clay Science.* 2003, in press.
- [1-8] Lee, R. W., Glater, J., Yoram, C., Martin, C., Kovac, K., Martin, N. M., and Dan, W. B. "Low-Pressure RO Membrane Desalination of Agricultural Drainage Water," *Desalination.* 155 (2003) 109.
- [1-9] Vercauteren, S., Luyten J., Leysen, R., Vansant, E.F. "Synthesis and characterization of a pillared clay membrane," *J. Membr. Sci.*, 119 (1996) 161.
- [10] Vercauteren, S., Vayer, M., Van Damme, H., Luyten, J., Letsen, R., Vansant, E.F. "The preparation and characterization of ceramic membranes with a pillared clay top layer," *Colloid. Surf. A: Physicochem. Eng. Aspect.*, 138 (1998) 367.

- [1-11] Molinard A., Vansant, E.F. "Controlled gas adsorption properties of various pillared clays," *Adsorption*. **1** (1995) 49.
- [1-12] Hu, Z.H., Zhu, H.Y., Vansant, E.F. "Separation of nitrogen and organic vapors by pillared clay-carbon composite membrane," *Sep. Technol.*, Ed. E.F. Vansant, Elsevier, Amsterdam, 1994, p567-571.
- [1-13] Jagota, S., Harmer, M. A., Lemon, M. F., Jagota, A., and McCrion, E. M. "Pillared Smectite Clay for Coating Ceramic-Matrix Composites," *J. Am. Ceram. Soc.*, 78 (1995) 2243.
- [1-14] Giese, R. F., and Costanzo, P. M. "Behavior of water on the surface of kaolin minerals," *Abstracts of Papers of the Am. Chem. Soc.*, 190 (1985) 38.
- [1-15] Wan, Y., J. Kwong, H. G. Brandes, and R. C. Jones. "Influence of Amorphous Clay-Size Materials on Soil Plasticity and Shrink-Swell Behavior," *J. Geotech. Geoenviron. Eng.*, (2002) 1026.
- [1-16] Zhu, H. Y., Vansant, E. F., and Lu, G. Q. "Development of Composite Adsorbents of Carbon and Intercalated Clay for N<sub>2</sub> and O<sub>2</sub> Adsorption: A Preliminary Study," *J. Colloid Interf. Sci.* 210 (1999a) 352.
- [1-17] Zhu, H. Y., Ma, Q., and Lu, G. Q. "Influence of heat treatment on the pore and adsorption characteristics of sodium doped alumina pillared bentonite," *J. Porous Mat.* 6 (1999b) 135.
- [1-18] Valverde, J. L., Canizares, P., Sun Kou, M. R., and Molina, C. B. "Enhanced Thermal Stability of Al-pillared Smectites Modified with Ce and La," *Clays and Clay M Mineral.* **48** (2000) 423.

## CHAPTER 2

### Desalination by Reverse Osmosis Using MFI Zeolite Membranes

This chapter reports on reverse osmosis desalination of aqueous solutions using  $\alpha$ -alumina-supported MFI-type zeolite membranes. At steady state, a  $\text{Na}^+$  rejection of 76.7% with a water flux of about  $0.112 \text{ kg m}^{-2} \text{ h}^{-1}$  was obtained for a 0.1 M NaCl feed solution under an applied pressure of 2.07 MPa. For a complex feed solution containing 0.1M NaCl+0.1M KCl+0.1M  $\text{NH}_4\text{Cl}$ +0.1M  $\text{CaCl}_2$ +0.1M  $\text{MgCl}_2$ , rejections of  $\text{Na}^+$ ,  $\text{K}^+$ ,  $\text{NH}_4^+$ ,  $\text{Ca}^{2+}$ , and  $\text{Mg}^{2+}$  reached 58.1%, 62.6%, 79.9%, 80.7%, and 88.4%, respectively, with a stabilized water flux of  $0.058 \text{ kg m}^{-2} \text{ h}^{-1}$ , after 145 hours of operation at an applied pressure of 2.4 MPa.

#### 2.1 Introduction

Zeolite membranes have been studied extensively for more than fifteen years, mainly focusing on gas separation and liquid pervaporation processes. Recently, molecular dynamic simulation has shown that zeolite membranes are theoretically suitable for ion removal from aqueous solutions by reverse osmosis (RO) processes. <sup>[2-1]</sup> The simulation revealed that 100%  $\text{Na}^+$  rejection could be achieved on a perfect (single crystal), all-Si, ZK-4 membrane through RO. The separation mechanism of the perfect ZK-4 zeolite membranes is the size exclusion of hydrated ions, which have kinetic sizes (0.8~1.0 nm for  $[\text{Na}(\text{H}_2\text{O})_x]^+$ )<sup>[2-2]</sup> significantly larger than the aperture of the ZK-4 zeolite (diameter 0.42 nm). Kumakiri et al. <sup>[2-3]</sup> reported using an A-type zeolite membrane in RO separation of water/ethanol mixtures. The hydrophilic A-type zeolite (pore size ~0.4nm) membranes showed 44% rejection of ethanol and a water flux of  $0.058 \text{ kg} \cdot \text{m}^{-2} \cdot \text{h}^{-1}$  under an applied feed pressure of 1.5 MPa. However, experimental demonstration of RO desalination on zeolite membranes has not been reported so far.

Results of the computer simulation and experimental RO separation of water/ethanol mixtures on A-type membranes indicate that it may be possible for zeolite membranes to simultaneously separate ions and dissolved organic compounds from aqueous solutions by RO processes. Zeolite membranes may be used as an alternative to polymeric membranes for desalination of complex wastewaters, which contain organic solvents and radioactive elements, or when high temperature operation is desired. However, existing zeolite membranes possess an imperfect polycrystalline structure <sup>[2-4]</sup> and may be of different types with various pore sizes and Si/Al ratios. <sup>[2-5]</sup> Therefore, experimental investigation of the effectiveness of RO desalination using actual zeolite membranes is necessary. This work experimentally demonstrates RO separation using a  $\alpha$ -alumina-supported MFI-type zeolite membrane for solutions containing a single cation and multiple cations.

## **2.2 Experimental**

### **2.2.1 Materials and apparatus**

$\alpha$ -alumina supported MFI-type zeolite membranes (thickness  $\sim 3\mu\text{m}$ ) were synthesized through in-situ crystallization. The detailed synthesis procedure is available in the literature. <sup>[2-6, 7]</sup> The disc-shaped alumina substrates were 28 mm in diameter and 2 mm in thickness with an average pore size of  $0.1\mu\text{m}$  and porosity of about 35%. The composition of the synthesis solution was 20 g  $\text{SiO}_2$ +100 ml (1M) TPAOH+1.4 g NaOH+3.2 g  $\text{H}_2\text{O}$ . Hydrothermal treatment was conducted in an autoclave at  $180^\circ\text{C}$  with autogenous pressure for four hours. After synthesis, the membrane was washed and fired, and received a second hydrothermal treatment under the same conditions. After the second hydrothermal treatment the membrane was washed, dried, and then activated by calcining at  $450^\circ\text{C}$  for five hours. The membranes were characterized by X-ray diffraction (XRD) and scanning electron microscope (SEM), which showed results essentially identical to those in our previous reports. <sup>[2-4,7]</sup>

The RO separation system is shown schematically in Fig. 2-1. The zeolite membrane was mounted in a stainless steel cell sealed by silicone O-rings, facing the feed stream. Both the feed chamber and permeate chamber of the cell had similar small volumes of about 0.5 cm<sup>3</sup>. A porous stainless steel disc (pore diameter of 5 μm and thickness of 2 mm, Mott Co.) was placed underneath the alumina substrate to prevent the membrane from cracking under high pressure. The feed pressure was maintained by a nitrogen cylinder and the feed flow rate was controlled by a needle valve located at the feed chamber exit. In this series of experiments, the feed flow rate was 0.5 ml/min at outlet. The liquid permeate was collected by a small Teflon bottle at ambient pressure (86 kPa in Socorro, New Mexico). The sample bottle was connected to the gas phase of a water flask to prevent evaporation of the received liquid. Solute concentration was analyzed by a dual-column ion chromatograph (IC, DX120, Dionex) with a computer data acquisition and analysis system.

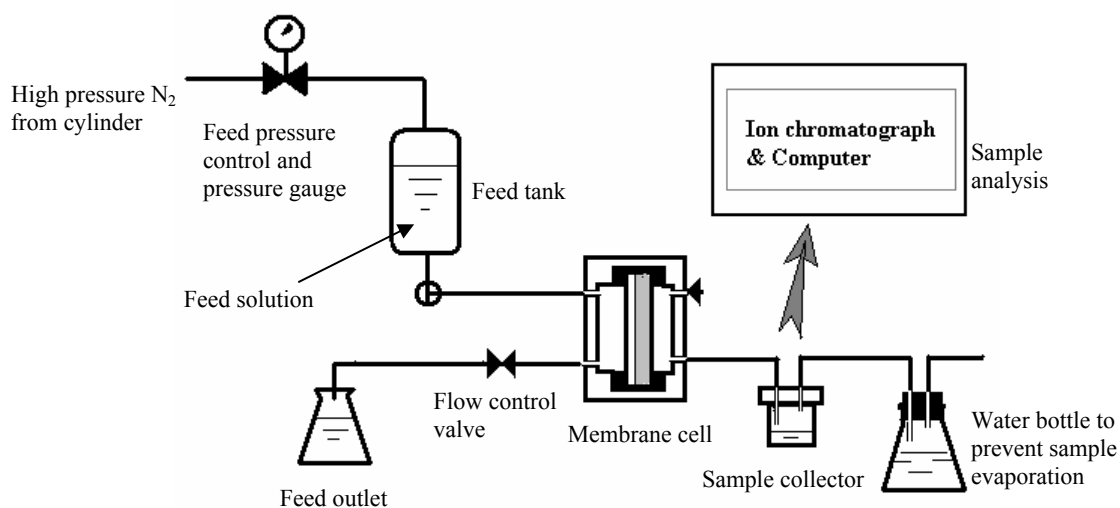


**Fig. 2-1.** Schematic diagram of the RO system.

Chemicals used in this study included tetrapropylammonium hydroxide (TPAOH, 1 M, Aldrich), sodium hydroxide (NaOH, 99.99%, Aldrich), fumed silica (99.98%, Aldrich), sodium chloride (Analytical

reagent, Riedel-deHaen), magnesium chloride (>99.0%, Alfa Aesar), calcium chloride (ACS reagent, ACROS), potassium chloride (Analytical reagent, J.T. Baker), ammonium chloride (ACS, >99.5%, Alfa Aesar) and deionized (DI) water. The feed solutions were prepared by dissolving the salts into the DI water. Thus, the anions of the solutions are  $\text{Cl}^-$  only.

### 2.2.2 Results and Discussions

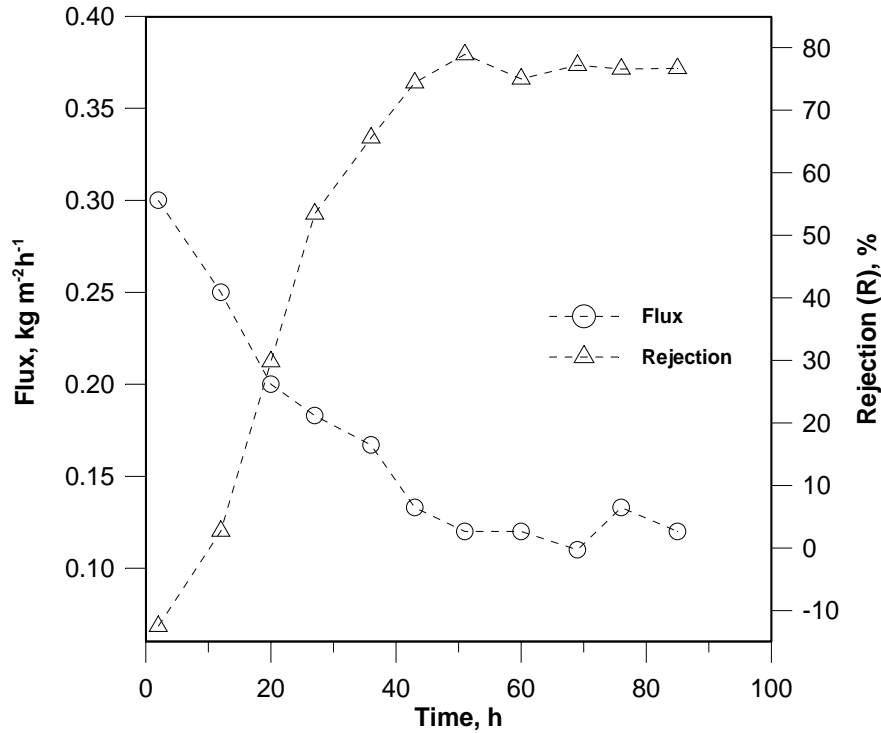
Reverse osmosis experiments were conducted at room temperature for a 0.1M NaCl solution and a multicomponent solution of 0.1M NaCl+0.1M KCl+0.1M  $\text{NH}_4\text{Cl}$ +0.1M  $\text{CaCl}_2$ +0.1M  $\text{MgCl}_2$ , respectively. Water flux and ion rejection were measured as functions of operation time. The time at which the first drop of liquid appeared in the sample collector was treated as the starting point (i.e.  $t = 0$  h) of the RO process. The definitions of water flux ( $F$ , not corrected by substrate porosity) and ion rejection ( $R$ ) are as follows:

$$F = \frac{Q_w}{A_m \cdot \Delta t} \quad (2-1)$$

$$R = \frac{(C_s)_{feed} - (C_s)_{perm}}{(C_s)_{feed}} \times 100\% \quad (2-2)$$

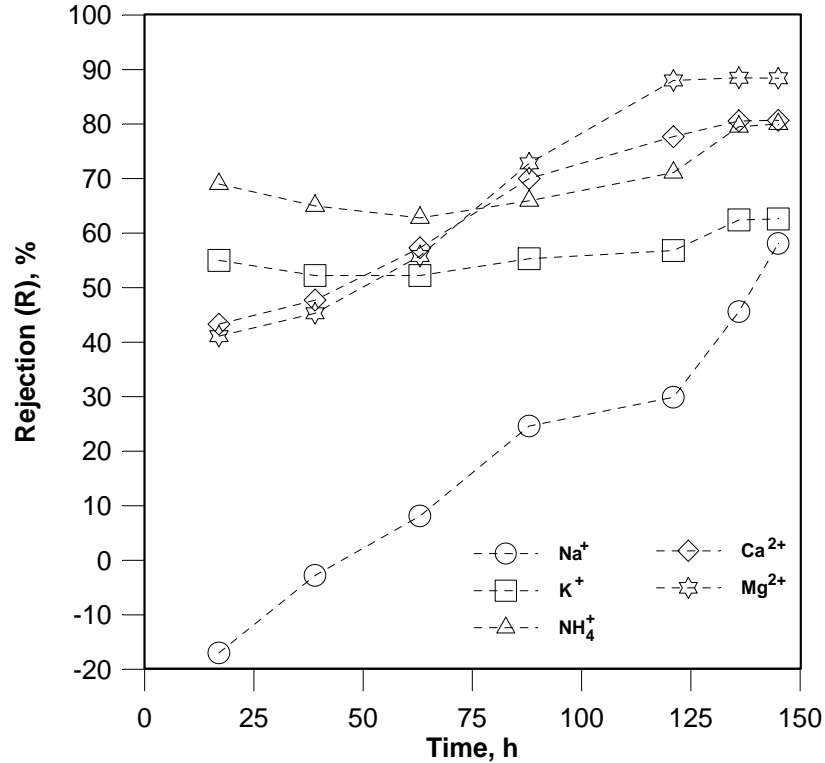
where  $(C_s)_{feed}$  and  $(C_s)_{perm}$  are cation concentrations of the feed and permeate solutions, respectively;  $Q_w$  is the quantity of water collected in time period  $\Delta t$ ; and  $A_m$  is the effective membrane area,  $2.5 \times 10^{-4} \text{ m}^2$  in this case.

Figure 2-2 shows the rejection and water flux values versus RO operation time for the 0.1M NaCl feed solution. Reverse osmosis was conducted at a feed side pressure of 2.07 MPa (gauge). Within the first 50 hours of permeation, water flux decreased while  $\text{Na}^+$  rejection increased with time. After 50 hours, water flux and ion rejection tended to stabilize at  $0.12 \text{ kg m}^{-2} \text{ h}^{-1}$  and 77%, respectively.



**Fig. 2-2.** Water flux and Na<sup>+</sup> rejection as functions of OR operation time for the 0.1M NaCl solution.

Figure 2-3 shows ion rejection values versus RO operation time for a feed solution containing multiple types of cations, including Na<sup>+</sup>, K<sup>+</sup>, NH<sub>4</sub><sup>+</sup>, Ca<sup>2+</sup>, and Mg<sup>2+</sup>. Reverse osmosis was conducted at a feed side pressure of 2.4 MPa (gauge). In this case, water flux dropped from an initial value of 0.121 kg m<sup>-2</sup> h<sup>-1</sup> to a stabilized value of 0.058 kg m<sup>-2</sup> h<sup>-1</sup> in about 17 hours. Cation rejection had a similar trend of increasing then stabilizing throughout the operation time except for the rejection of Na<sup>+</sup>, which did not equilibrate within the operation time period. After 145 hours of permeation, rejection of Na<sup>+</sup>, K<sup>+</sup>, NH<sub>4</sub><sup>+</sup>, Ca<sup>2+</sup>, and Mg<sup>2+</sup> reached 58.1%, 62.6%, 79.9%, 80.7%, and 88.4%, respectively.



**Fig. 2-3.** Ion rejection as a function of operation time for the multicomponent feed solution containing 0.1M NaCl, 0.1M KCl, 0.1M NH<sub>4</sub>Cl, 0.1M CaCl<sub>2</sub>, and 0.1M MgCl<sub>2</sub>.

The Na<sup>+</sup> rejection values were negative during the first two hours for the 0.1M-NaCl-solution and during the first 40 hours for the multicomponent solution. These abnormal results were likely caused by dissolution of the synthesis materials trapped in the substrate, because such negative rejections were not observed for the other four cations. Due to the extremely high concentrations of NaOH and SiO<sub>2</sub> in the membrane synthesis solution, significant amounts of Na<sup>+</sup> might have been trapped in the substrate and the zeolite intercrystal pores that formed low-solubility Na<sub>2</sub>SiO<sub>3</sub> and/or Na[Al(SiO<sub>3</sub>)<sub>2</sub>] during firing. These sodium aluminosilicate compounds cannot be cleaned thoroughly by regular rinsing and leaching processes because it is difficult to fill up with water in the submicron pores near the membrane/substrate contacting area. The Na<sup>+</sup>, however, could dissolve slowly into the permeate water during the RO process that caused the negative rejection values in the initial period of operation.

The decline of water flux and the increase in ion rejection with permeation time may be explained by the following analysis based on the microstructure and surface property of the zeolite membrane. For the MFI zeolite, which has an aperture size of 0.55 nm, molecular species as large as 0.84 nm of kinetic diameter (e.g. triisopropylbenzene) can still get into the zeolite channels but its mobility in the zeolitic pores is extremely low ( $\sim 10^{-14}$  cm<sup>2</sup>/s).<sup>[2-8]</sup> Therefore, it is possible that some hydrated ions could have entered the zeolitic pores that hindered the diffusion of water molecules and thus reduced the water flux. On the other hand, the zeolite membrane is a polycrystalline film, which inevitably contains intercrystal pores of nanometer size.<sup>[2-4]</sup> These intercrystal pores/boundaries may allow the sub-nanometer-sized hydrated ions to pass in the beginning. However, along the time, overlapping double layers may develop in the microporous intercrystal boundaries due to ion adsorption on the external surface of the zeolite crystals. The overlapping double-layers can restrict ion transport while allowing electrically neutral species to enter freely.<sup>[2-9]</sup>

## 2.3 Conclusions

Reverse osmosis of aqueous solutions on MFI zeolite membranes was experimentally demonstrated in this study. High rejection values were obtained for a concentrated solution containing five different types of cations, including Na<sup>+</sup>, K<sup>+</sup>, NH<sub>4</sub><sup>+</sup>, Ca<sup>2+</sup>, and Mg<sup>2+</sup>. Results of this work show that zeolite membranes have great potential for applications in RO desalination of complex mixtures. The zeolite membranes, due to their excellent chemical and thermal stabilities, may be particularly useful for treating various kinds of wastewater that cannot be handled effectively by polymeric RO membranes, such as solutions containing organic solvents and radioactive ions and/or those requiring operation at elevated temperatures. However, fundamental studies are needed to understand the mechanisms of the RO processes on the polycrystalline membranes and the effects of microstructure and chemistry of the zeolite membranes on RO performance.

## 2.4 References

- [2-1] Lin, J. and Murad, M. A.: "A Computer Simulation Study of the Separation of Aqueous Solution Using Thin Zeolite Membranes," *Molec. Phys.* (2001) **99**, 1175.
- [2-2] Murad, ] M. A., Oder, S. K., and Lin, J.: "Molecular Simulation of Osmosis, Reverse Osmosis, and Electro-Osmosis in Aqueous and Methanolic Electrolyte Solutions," *Molec. Phys.* (1998) **95**, 401.
- [2-3] I. T. Kumakiri, Yamaguchi, and S. I. Nakao: "Application of a Zeolite A Membrane to Reverse Osmosis Process," *J. Chem. Eng. Jpn.* (2000) **33**, 333.
- [2-4] J. Dong, J., et al.: "Template Removal Associated Microstructural Development of Ceramic Supported MFI Zeolite Membranes," *Micropor. Mesopor. Mat.* (2000) **34**, 241.
- [2-5] Caro, J.M., Noack, Kolsch, P., and Schafer, R.: "Zeolite Membranes—State of Their Development and Perspective," *Micropor. Mesopor. Mat.* (2000) **38**, 3.
- [2-6] Vroon, Z.A.E.P. "Synthesis and Transport Properties of Thin Ceramic Supported Zeolite (MFI) Membranes," PhD Dissertation, University of Twente, The Netherlands, (1995).
- [2-7] Dong, J., Wegner, K. and Lin, Y.S.: "Synthesis of Submicron Silicalite Membranes on Porous Ceramic Supports," *J. Membrane Sci.*, (1998) **148**, 233.
- [2-8] Ruthven, D. M.: *Principles of Adsorption and Adsorption Processes*. John Wiley & Sons, New York, (1984).
- [2-9] Malusis, M,A., and Shackelford, C.D.: "Chemico-Osmotic Efficiency of a Geosynthetic Clay Liner," *J. Geotech. Geoenviron. Eng.*, (2000) **128**, 629.

## CHAPTER 3

### Reverse Osmosis of Ionic Aqueous Solutions on A MFI Zeolite Membrane; A Study of Salt Rejection Mechanisms

Separation of ions from aqueous solutions was performed by reverse osmosis (RO) on an  $\alpha$ -alumina-supported MFI-type zeolite membrane synthesized by in-situ crystallization. For the 0.1M chloride single-salt solutions, the separation efficiency in terms of ion rejection was found to increase with the ion valence in the order  $r_{Al^{3+}} > r_{Mg^{2+}} > r_{Na^+}$ , while the ion and water fluxes changed in the reverse order. The charge density, size, and apparent dynamic hydration number of the ion as well as the mobility of the hydrated ion were found to have critical influences on ion diffusion and water permeation through the polycrystalline zeolite membrane.

#### 3.1 Introduction

Zeolites are microporous aluminosilicate crystalline materials, which have been widely used as adsorbents for gas and liquid separations due to their extremely uniform pore size and unique surface properties. In the past two decades, various types of supported polycrystalline zeolite membranes have been developed on different substrates with minimized intercrystal pores. [3-1,2] The zeolite membranes were extensively researched for many industry-relevant separations via gas permeation and liquid pervaporation processes. The general separation mechanisms on zeolite membranes include molecular sieving and competitive adsorption and diffusion. [3-3-6]

Recently, the possibility of using zeolite membranes to remove ions from aqueous solutions by reverse osmosis (RO) has been explored by molecular dynamic (MD) simulation [3-7]. The result of MD simulation has shown complete rejection of  $Na^+$  on a perfect all-Si ZK-4 membrane by size exclusion of the hydrated ions with the complex sizes much larger than the zeolitic pore size (~0.42 nm). Reverse osmosis desalination by zeolite membranes may offer an alternative for some difficult water treatment

processes such as concentration of low-level radioactive wastewater and desalination of organic-containing, high-concentration produced water from oil and gas operations, where the conventional technologies, including polymeric RO membranes, are either inapplicable or inefficient.

Kumakiri and coworkers<sup>[3-8]</sup> reported a 44% rejection of ethanol from its aqueous solution by RO on a zeolite-A membrane with a total flux of  $0.058 \text{ kg}\cdot\text{m}^{-2}\cdot\text{h}^{-1}$  under an applied pressure of 1.5MPa. More recently, we have demonstrated desalination of single-salt and multicomponent-ionic solutions on MFI-type zeolite (pore size 0.56nm) membranes.<sup>[3-9]</sup> At steady state, a  $\text{Na}^+$  rejection of 76.7% with a water flux of about  $0.112 \text{ kg m}^{-2} \text{ h}^{-1}$  was obtained for a 0.1M NaCl feed solution under a transmembrane pressure of 2.07 MPa. For a complex feed solution containing 0.1M NaCl+0.1M KCl+0.1M  $\text{NH}_4\text{Cl}$ +0.1M  $\text{CaCl}_2$ +0.1M  $\text{MgCl}_2$ , rejections of  $\text{Na}^+$ ,  $\text{K}^+$ ,  $\text{NH}_4^+$ ,  $\text{Ca}^{2+}$ , and  $\text{Mg}^{2+}$  were 58.1%, 62.6%, 79.9%, 80.7%, and 88.4%, respectively, with a stabilized water flux of  $0.058 \text{ kg m}^{-2} \text{ h}^{-1}$  under an applied pressure of 2.4 MPa. The decrease in  $\text{Na}^+$  rejection with an increase in the ionic strength indicates the existence of ion permeation through paths other than the zeolitic pores since the hydrated-ion sizes are virtually independent of the ion concentration.<sup>[3-10]</sup> Therefore, the size exclusion mechanism is insufficient to describe the real membrane process.

Polycrystalline zeolite membranes usually contain two types of pores, i.e. the uniform subnanometer zeolitic pores and intercrystal micropores with size distribution.<sup>[3-11,12]</sup> It is understood that the intercrystal pores significantly lower the gas separation performance of zeolite membranes. Therefore, to further develop RO technology on zeolite membranes, it is necessary to investigate the mechanisms of ion and water transport in actual membranes. In this study, the effects of charge density, size, and hydration number of the ion on RO performance were investigated on a MFI-type zeolite membrane.

## 3.2 Experimental

### 3.2.1 Materials and Chemicals

Chemicals used in this study included tetrapropylammonium hydroxide (TPAOH) (1M solution, Aldrich), sodium hydroxide (NaOH) (99.99%, Aldrich), fumed silica (SiO<sub>2</sub>) (99.98%, Aldrich), sodium chloride (NaCl) (Analytical reagent, Riedel-deHaen), magnesium chloride (MgCl<sub>2</sub>) (>99.0%, Alfa Aesar), calcium chloride (CaCl<sub>2</sub>) (ACS reagent, ACROS), potassium chloride (KCl) (“Baker Analyzed” reagent, J.T. Baker), aluminum chloride (AlCl<sub>3</sub>) (99.0%, Aldrich), and deionized (DI) water.

### 3.2.2 Membrane Synthesis

$\alpha$ -alumina supported MFI-type zeolite membranes (thickness  $\sim 3\mu\text{m}$ ) were synthesized by the in-situ crystallization method. The detailed membrane synthesis procedure is available in the literature<sup>[3-13,14]</sup>. The disc-shaped alumina substrates were 28 mm in diameter and 4 mm thick with an average pore size of  $\sim 0.15\mu\text{m}$  and a porosity of 35-40%. The composition of the zeolite membrane synthesis solution was 20g SiO<sub>2</sub>+100ml (1.0M) TPAOH+1.4g NaOH+3.2g H<sub>2</sub>O. Hydrothermal treatment was conducted in an autoclave at 180°C and autogenous pressure for four hours. After drying overnight at 50°C, the membrane was activated by calcining at 450°C in air for five hours. The membranes used in this study were obtained by a single hydrothermal treatment. The membranes were characterized by X-ray diffraction (XRD) and scanning electron microscope (SEM) and tested by a transient N<sub>2</sub> permeation before and after calcination. A defect-free membrane is impermeable for gases before removal of the TPA<sup>+</sup> template molecules, which occupy the zeolite channels. The as-synthesized membranes with N<sub>2</sub> permeance less than 10<sup>-10</sup> mol/m<sup>2</sup>·Pa·s were calcined and used in the RO experiments.

### 3.2.3 RO Experiment

Figure 3-1 shows the experimental system employed for the RO separation experiment. The zeolite membrane was mounted in a stainless steel cell with the membrane surface facing the feed stream. Both the feed side chamber and permeate side chamber of the cell had a small volume of about 0.5 cm<sup>3</sup>. The feed pressure was maintained by a nitrogen cylinder and the feed flow rate was controlled by a needle valve located at the exit of the feed chamber. In this study, the feed flow rate was 0.2 ml/min at the outlet. The liquid permeate was collected by an 8-ml Teflon bottle at atmospheric pressure. The whole membrane cell was immersed in a water bath ( $\pm 0.2^\circ\text{C}$ , RDL 20, GCA) for temperature control.

To prevent evaporation of the collected permeate liquid during the operation, the atmosphere in the sample collector was kept at 100% RH by connecting it to the vapor phase of another bottle of water through a Teflon tube. All the ion concentrations, except for that of the aluminum ion ( $\text{Al}^{3+}$ ), were analyzed by a dual-column ion chromatograph (IC, DX120, Dionex) with a computer workstation. The  $\text{Al}^{3+}$  concentration was measured by Flame Atomic Absorption (FAA) (Varian Model 110).

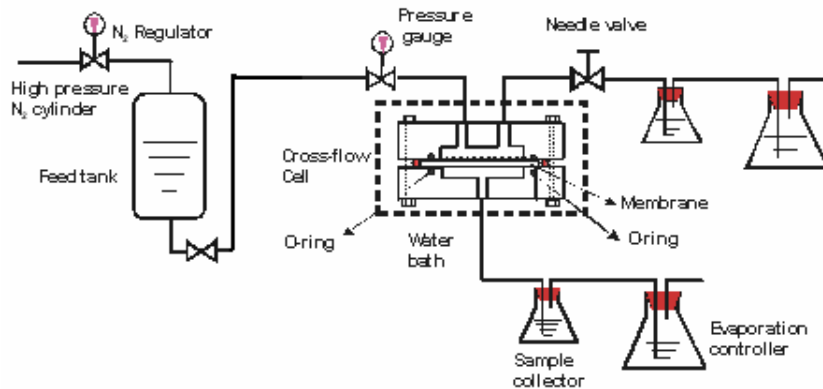


**Fig. 3-1.** Schematic diagram of the RO system.

The permeate sample was analyzed at a time interval of 12 hours. Rejection of ion  $i$ ,  $r_i$ , is defined by equation (3-1),

$$r_i = \frac{(C_i)_{feed} - (C_i)_{perm}}{(C_i)_{feed}} \times 100\% \quad (3-1)$$

where  $(C_i)_{feed}$  and  $(C_i)_{perm}$  are concentrations of ion  $i$  in the feed and permeate solutions, respectively. The water flux ( $F_w$ ) and permeance ( $P_a$ ) are defined as follows:

$$P_a = \frac{F_w}{\Delta P} = \frac{F_w}{P_f - P_p - \Delta\pi} \quad (3-2)$$

$$F_w = \frac{Q_w}{A_m \cdot t} \quad (3-3)$$

$$\Delta\pi = \left[ \left( \frac{C_s}{100 - C_s} \right)_{perm} - \left( \frac{C_s}{100 - C_s} \right)_{feed} \right] \frac{RT}{Mw} \quad (3-4)$$

where  $C_s$  is the total ion concentration;  $\Delta\pi$  is the difference of osmosis pressures between the feed and permeate solutions;  $Q_w$  is the quantity of water collected in a time period of  $t$ ;  $A_m$  is the effective membrane area;  $T$  is the temperature;  $R$  is the gas constant; and  $Mw$  is the molar weight of the cation.

### 3.3 Results

For all the solutions, it was observed that the water flux decreased while the ion rejection increased with time and both stabilized in 24 to 48 hours as no significant changes were observed afterwards. The time dependencies of flux and rejection observed in this study were similar to those in our previous report.<sup>[3-9]</sup> Water flux and ion rejection data presented in this paper are stabilized values obtained by averaging data of seven samples collected after the initial 48 hours. Only cation rejection and cation molar fluxes are reported in this article. However, the anion concentration in the permeate solutions was also determined. The measured cation/anion molar ratio in the permeate products matched the stoichiometric ratio of the constituent ions of the solutes, indicating permeation of paired-ions through

the zeolite membrane to maintain the electrical neutrality. Table 3-1 summarizes the results of RO separation for five single-salt solutions together with the permeation data of DI water.

**Table 3-1.** RO Separation Results for Single-Solute Solutions at 25°C

Solution	Pressure	Flux	Permeance	Rejection ( $r_i$ )
	MPa	kg·m <sup>-2</sup> ·h <sup>-1</sup>	kg·MPa <sup>-1</sup> ·m <sup>-2</sup> ·h <sup>-1</sup>	%
H <sub>2</sub> O (DI)	3.4	0.266	0.077	
0.10M NaCl	2.1	0.162	0.078	21.6
0.10M KCl	2.1	0.174	0.084	21.9
0.10M MgCl <sub>2</sub>	2.1	0.081	0.039	68.6
0.10M CaCl <sub>2</sub>	2.1	0.096	0.046	57.6
0.10M AlCl <sub>3</sub>	2.1	0.057	0.028	96.2

### 3.4 Discussion

The MFI-type zeolite has an effective intracrystal pore diameter of 0.56 nm, which is smaller than the sizes of hydrated ions involved in the current systems. Table 3-2 lists the hydration numbers and crystallographic sizes of the ions. A nearly perfect ion separation may be achieved on a perfect membrane (i.e. containing zeolitic pores only), as predicted by MD simulation.<sup>[3-7]</sup> However, on a real membrane, transport of hydrated ions exists in the intercrystal pores that are larger than the hydrated ions, as illustrated in Fig. 3-2. Moreover, ions may also diffuse through the zeolite channels by ion exchange on the feed side and ion leaching at the permeate side since the alumina supported membrane is not pure silicalite even though the synthesis solution is aluminum-free.<sup>[3-14]</sup> Nevertheless, ion leaking through the zeolitic pores is likely to be minor since the membrane has a very high Si/Al ratio; thereby, having a minimum capacity of ion exchange.

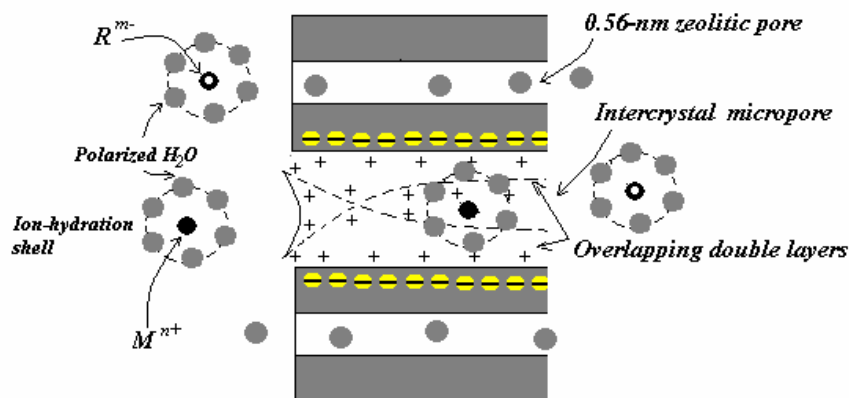


**Fig. 3-2.** Schematic illustration of the water and ion transport through a polycrystalline MFI membrane containing zeolitic pores and larger intercrystal pores.

Complete rejection of hydrated ions can occur on a perfect membrane with no intercrystal pores and other microdefects only if the hydration shell is rigid and all the water molecules in the first shell are tightly bound with the ion during diffusion. It is understood that the attachment of water molecules to the ion has a lifetime, which depends on the type of ion.<sup>[3-15-17]</sup> Experiments with an aqueous, size exclusion ion chromatograph showed that only a portion of the water molecules in the first hydration shell is tightly bound with the ion during diffusion.<sup>[3-18]</sup> The apparent dynamic hydration number (ADHN) is used to denote the number of tightly bound water molecules and distinguish it from the equilibrium hydration number in solution. According to the dynamic ionic size with ADHN (see Table 3-2), complete ion rejection by size exclusion is not possible on the MFI membrane for the current ions except for the hydrated  $Al^{3+}$ . Small ions like  $Na^+$ ,  $K^+$  and  $Cl^-$  may be able to enter the 0.56-nm zeolite channels but their diffusivities are expected to be extremely low due to the strong effect of zeolite framework on the charged ions in the cages.

**Table 3-2.** Hydration Numbers (in the First Shell), Experimental ADHN, and Sizes of the Ions Involved in This Study <sup>[3-18]</sup>

Ion	Crystal ion size (dia.), nm	Hydration number in the first shell	ADHN	Dynamic ion size with ADHN
Na <sup>+</sup>	0.204	6	0.30	0.366
K <sup>+</sup>	0.276	6	---	0.420
Mg <sup>2+</sup>	0.144	6	5.85	0.600
Ca <sup>2+</sup>	0.246	10	2.09	0.506
Al <sup>3+</sup>	0.108	6	8.68	0.674
Cl <sup>-</sup>	0.362	6	---	0.390

Ion transport through the intercrystal pores with charged surfaces are restricted by the overlapping charged double layers. <sup>[3-19-21]</sup> The average size of the intercrystal pore is usually nanometer- or subnanometer-scale in randomly oriented MFI membranes with reasonable quality. <sup>[3-11,12]</sup> Although aluminum-free synthesis solutions were used, the alumina-supported MFI membranes were not aluminum-free in their frameworks. A small amount of aluminum can incorporate into the zeolite framework due to slight dissolution of the alumina surface in the high-pH synthesis solution and solid state diffusion of Al<sup>3+</sup> during the calcination process. <sup>[3-14]</sup> The substitution of Si<sup>4+</sup> with Al<sup>3+</sup> ions creates negative charges on the zeolite surface, which forms charged double layers in the porous structure when contacting liquid water. For a specific membrane, the ion rejection and water flux depend not only on the size and charge density of the solute ion but also on the double layer thickness, which is a function of the ionic strength and temperature of the aqueous solution. <sup>[3-22]</sup>

The RO results given in Table 3-1 are reorganized and represented in Figs. 3-3 and 3-4. Figure 3-3 shows that the ion and water fluxes decrease and the ion rejection increases in the order of 0.1M NaCl, 0.1M MgCl<sub>2</sub>, and 0.1M AlCl<sub>3</sub>. The reduction of ion transport is caused by the increasing charge density, which enhances the interactions between the ions and the pore wall and double layers. Moreover, the

apparent dynamic hydration number also increases with the charge density in the order of  $\text{Na}^+ < \text{Mg}^{2+} < \text{Al}^{3+}$  (see Table 3-2). Since the intercrystal pores have a size distribution, the number of intercrystal pores permeable for ions is inversely proportional to the hydrated ion size or ADHN. Therefore, ion rejection increases in the order of  $\text{Na}^+$ ,  $\text{Mg}^{2+}$ , and  $\text{Al}^{3+}$ .

The mobility of water molecules neighboring the ions decreases with the increase of the ion-water bond and the dielectric friction, which enhance with the ion charge density and the inverse ion radius [3-18, 23-25]. In the micropores, free water molecules are much fewer than those in the bulk solution because the hydrated ions interact directly with the charged double layer, especially when the double layers tend to overlap in a small space. [3-21] Thus, the mobility of water molecules inside the pores is lower than that in the bulk solution because of the joint motion of water and ion [3-18] under the influence of charged double layers. Therefore, water and ion fluxes decrease in the order of  $\text{Na}^+$ ,  $\text{Mg}^{2+}$ , and  $\text{Al}^{3+}$ .

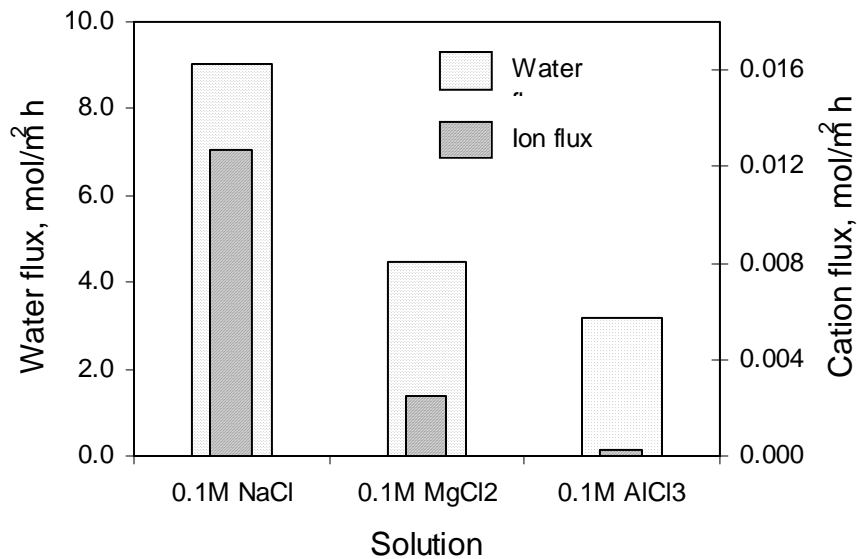


**Fig. 3-3.** Effect of cation valance on water and ion fluxes.

Figure 3-4 shows the comparisons of ion and water fluxes for ions with different crystal sizes but the same valences. The ion and water fluxes for the 0.1M NaCl solution were lower than those for the 0.1M KCl solution. This can be explained by the fact that, for alkali ions in aqueous solutions, the

diffusion coefficient increases and the friction coefficient decreases with increasing crystallographic ion size.<sup>[3-26,27]</sup> The rejections of Na<sup>+</sup> and K<sup>+</sup> were close because they have a similar hydrated ion size (with ADHN). Similar results were obtained by comparing the ion and water fluxes between the MgCl<sub>2</sub> and CaCl<sub>2</sub> 0.1M solutions. However, the rejection rate of Mg<sup>2+</sup> was much higher than that of Ca<sup>2+</sup> (see Table 3-1) because the former has a stronger polarization effect on the surrounding water molecules<sup>[3-28]</sup> and possesses a higher ADHN.<sup>[3-18]</sup>

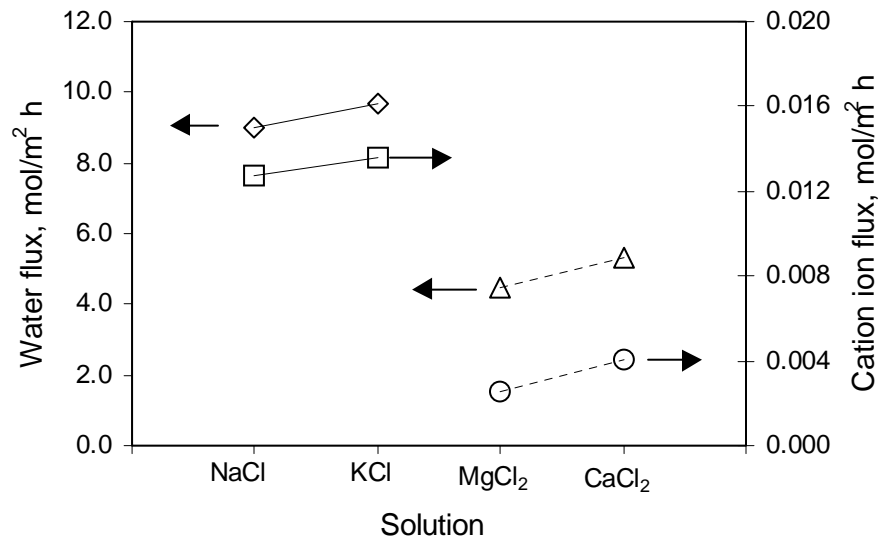


**Fig. 3-4.** Effect of cation size on water and ion fluxes.

### 3.5 Conclusions

Ion separation by RO through an alumina-supported MFI membrane was investigated for a number of single-salt solutions. The ion rejection and water flux were found to depend on the charge density of the ion and the dynamic size and diffusivity of the hydrated ion. The randomly oriented MFI polycrystalline membrane contains two types of pores, i.e. the uniform 0.56-nm diameter zeolite channels and microporous intercrystal pores with a size distribution at nanometer scale. The experimental results

indicate that different mechanisms control the transport of ion and water molecules through the intracrystal zeolite channels and the intercrystal pores. Ion rejection on the zeolitic channel is controlled by a size exclusion effect on the large hydrated ions. Ion separation through the intercrystal micropores is caused by the strong interaction between the ion and the charged double layers. The ion–double layer interaction restricts ion diffusion in the microporous space.

### 3.6 References

- [3-1] Caro, J. Noack, M., Kolsch, P., and Schafer, R.: “Zeolite Membranes - State Of Their Development and Perspective.” *Micropor. Mesopor. Mat.* (2000) **38**, 3-24.
- [3-2] Lin, Y.S., Kumakiri, I., Nair, N.B. and Alsyouri, H.: “Microporous Inorganic Membranes,” *Sep. Purif. Method.* (2002) **31**, 229-379.
- [3-3] Liu, Q., Noble, R.D., Falconer, J.L., and Funkel, H.H.: “Organics/Water Separation by Pervaporation with a Zeolite Membrane.” *J. Membr. Sci.* (1996) **117**, 163–174.
- [3-4] Kusakabe, K., Kuroda, T., and Morooka, S.: “Separation of Carbon Dioxide from Nitrogen Using Ion-Exchanged Faujasite-Type Zeolite Membranes Formed on Porous Support Tubes,” *J. of Membrane Sci.* (1998) **148**, 13-23.
- [3-5] Dong, J., Liu, W., and Lin, Y.S.: “Hydrogen/Hydrocarbon Separation with MFI-Type Zeolite Membranes on Porous  $\alpha$ -Alumina Supports,” *AIChE J.* (2000a) **46**, 1957-1966.
- [3-6] Lai, Z. et al.: “Microstructural Optimization of a Zeolite Membrane for Organic Vapor Separation.” *Science* (2003) **300**, 456-460.
- [3-7] J. Lin and S. Murad. “A Computer Simulation Study of the Separation of Aqueous Solution Using Thin Zeolite Membranes,” *Molec. Phys.* (2001) **99**, 1175.
- [3-8] Kumakiri, I., Yamaguchi, T., and Nakao, S.I.: “Application of a Zeolite A Membrane to Reverse Osmosis Process,” *J. Chem. Eng. Jpn.* (2000) **33**, 333.

- [3-9] Li, L., Dong, J., Nenoff, T.M., and Lee, R.: "Desalination by Reverse Osmosis Using MFI Zeolite Membranes," *J. Membr. Sci.* (2003) submitted.
- [3-10] Chowdhuri, S. and Chandra, A.: "Molecular Dynamic Simulations of Aqueous NaCl and KCl Solutions: Effects of Ion Concentration on the Single-Particle, Pair, and Collective Dynamical Properties of Ions and Water Molecules," *J. Chem. Phys.* (2001) **115**, 3732-3741.
- [3-11] Yan, Y., Davis, M.E., and Gavalas, G.R.: "Preparation of Highly Selective Zeolite ZSM-5 Membranes by a Post-Synthetic Coking Treatment," *J. of Mem. Sci.* (1997) **123**, 95-103
- [3-12] Dong, J. et al.: "Template Removal Associated Microstructural Development of Ceramic Supported MFI Zeolite Membranes," *Micropor. Mesopor. Mat.* (2000b) **34**, 241.
- [3-13] Vroon, Z.A.E.P., Keizer, K. Burggraaf, A.J., and Verweij, H.: "Preparation and Characterization of Thin Zeolite MFI Membranes on Porous Supports," *J. Membr. Sci.* (1998) **144**, 65.
- [3-14] Dong, J., Wegner, K., and Lin, Y.S.: "Synthesis of Submicron Silicalite Membranes on Porous Ceramic Supports," *J. Membr. Sci.* (1998) **148**, 233-241.
- [3-15] Impey, R. W., Madden, P.A., and McDonald, I.R.: "Hydration and Mobility of Ions in Solution," *J. Phys. Chem.* (1983), **87**, 5071-5083.
- [3-16] Neilson, G.W. and Enderby, J.E.: "The Coordination of Metal Aquaions," *Adv. Inorg. Chem.* (1989) **34**, 195-218.
- [3-17] Helm, L., and Merbach, A.E.: "Water Exchange on Metal Ions: Experiments and Simulations," *Coord. Chem. Rev.* (1999) **187**, 151-181.
- [3-18] Kiriukhin, M. Y. and Collins, K.D.: "Dynamic Hydration Numbers for Biologically Important Ions," *Biophys. Chem.* (2002) **99**, 155-168.
- [3-19] Yousif, K. K. and Frederick, A. F. B.: "Simultaneous Flow of Water and Solutes through Geological Membranes-I Experimental Investigation," *Geochimica et Cosmochimica Acta.* (1973) **37**, 2577.

- [3-20] Ishiguro, J., Matsuura, T., and Detellier, C.: “Reverse-Osmosis Separation for a Montmorillonite Membrane,” *J. of Membrane Sci.* (1995) **107**, 8.
- [3-21] Yang, K.L., Yiacomini, S., and Tsouris, C.: “Monte Carlo Simulations of Electrical Double-Layer Formation in Nanopores,” *J. of Chem. Phys.* (2002) **117**, 8499-8507.
- [3-22] Huheey, J. E., Keiter, E.A., and Keiter, R.L.: *Inorganic Chemistry: Principles of Structure and Reactivity*. HarperCollins College Publisher, New York (1993).
- [3-23] Hubbard, J., and Onsager, L.: “Dielectric Dispersion and Dielectric Friction in Electrolyte Solutions. I.” *J. Chem. Phys.* (1977) **67**, 4850-4857.
- [3-24] Pavlov, M., Siegbahn, E.M., and Sandstrom, M.: “Hydration of Beryllium, Magnesium, Calcium, and Zinc Ions Using Density Functional Theory.” *J. Phys. Chem. A.* (1998) **102**, 219-228.
- [3-25] Biswas, R. and Bagchi, B.: “Ionic Mobility in Alcohols: From Dielectric Friction to Solvent-Berg Model,” *J. Chem. Phys.* (1997) **106**, 5587-5598.
- [3-26] Chong, S. and Hirata, F.: “Dynamics of Ions in Liquid Water: An Interaction-Site-Model Description,” *J. Chem. Phys.* (1999) **111**, 3654-3667.
- [3-27] Chowdhuri, S. and Chandra, A.: “Hydration Structure and Diffusion of Ions in Supercooled Water: Ion Size Effects,” *J. Chem. Phys.* (2003) **118**, 9719-9725.
- [3-28] Bak, I., Hutter, J., and Palinkas, G.: “Car-Parrinello Molecular Dynamics Simulation of the Hydrated Calcium Ion,” *J. Chem. Phys.* (2002) **117**, 9838-9843.

**CHAPTER 4**  
**Zeolite Membrane Reverse Osmosis Desalination of Produced Water**  
**from Oil and Gas Field Operations**

Actual produced water samples were taken from local oil and gas fields. All the produced water samples were first filtered through 0.7µm Whatman® filter paper to remove suspended solids. The filtered water was pre-treated with a 1.0% weight percent 20-40 mesh Darco® granular active carbon for 24 hours to remove the dissolved hydrocarbons. The granular activated carbon was removed by filtering with 0.7µm and 0.45µm filter papers. Table 4-1 and Table 4-2 give the compositions of the pre-treated gas- and oil-field produced water samples, which were used for reverse osmosis (RO) testing on a MFI zeolite membrane.

**Table 4-1.** Composition of Gasfield Produced Water (pH = 7.25) (Farmington, New Mexico)

Component	Concentration
Bicarbonate	790 ppm
Fluoride	222.7 ppm
Chloride	9802 ppm
Sulfate	522 ppm
Sodium	6396 ppm
Potassium	523 ppm
Magnesium	124 ppm
Calcium	185 ppm
Organic	(removed)
Total Dissolved Solids	18,300 ppm

**Table 4-2.** Composition of Oilfield Produced Water (pH = 6.98) (Hobbs, New Mexico)

Component	Concentration
Bicarbonate	820 ppm
Chloride	106,560 ppm
Sulfate	3,720 ppm
Sodium	66,630ppm
Potassium	593 ppm
Magnesium	654 ppm
Calcium	2511 ppm
Bromide	93 ppm
Organic	(removed)
Total Dissolved Solids	181,600 ppm

#### **4.1 Results of Desalination for Actual Produced Water**

The separation experiments are conducted at room temperature. The permeate was collected at a time interval of ~24 hours. Concentrations of cation and anion in both the permeate and the feed solution were analyzed by a dual column ion chromatograph (IC, Dionex, DX-120). A Six Cation-II standard and a Five Anion standard (Dionex) were used for calibration of cations and anions, respectively. The results of reverse osmosis testing of the two produced water samples are summarized in Table 4-3. Detailed separation data for the actual produced water are presented and discussed below.

**Table 4-3.** Summary of RO Desalination Results on the MFI Membrane

Sample	TDS (mg/l)	Operation pressure (MPa)	Flux (kg/(m <sup>2</sup> .h))	Overall Rejection* (%)
Gasfield	1.83×10 <sup>4</sup>	4.1	0.022	83.3
Oilfield	1.82×10 <sup>5</sup>	5.5	0.018	18.0

\* Definition of ion rejection:  $r_i = \frac{(C_i)_{feed} - (C_i)_{perm}}{(C_i)_{feed}} \times 100\%$

#### 4.1.1. Desalination of Gasfield Produced Water from Farmington, New Mexico

Figure 4-1 presents cation rejection as a function of operation time. The rejection of Ca<sup>2+</sup> and Mg<sup>2+</sup> ions was as high as 95% and rejection of Na<sup>+</sup> and K<sup>+</sup> was about 76~77%. The high rejection rate did not change with operation time. Anion rejection was also determined. The overall rejection of anion was in agreement with the rejection of cation. The flux was, however, found to be lower than those previously obtained for the simulated solutions (Fig. 4-3).

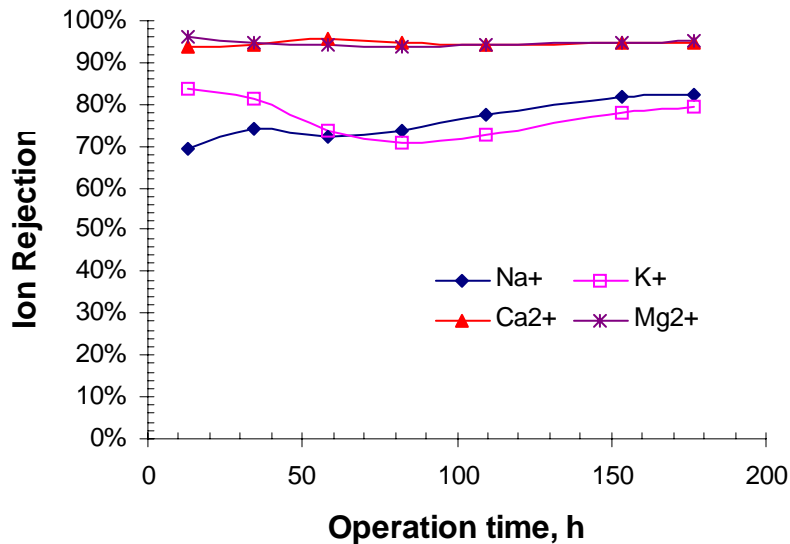


**Fig. 4-1.** Cation rejection as a function of operation time for the gasfield produced water.

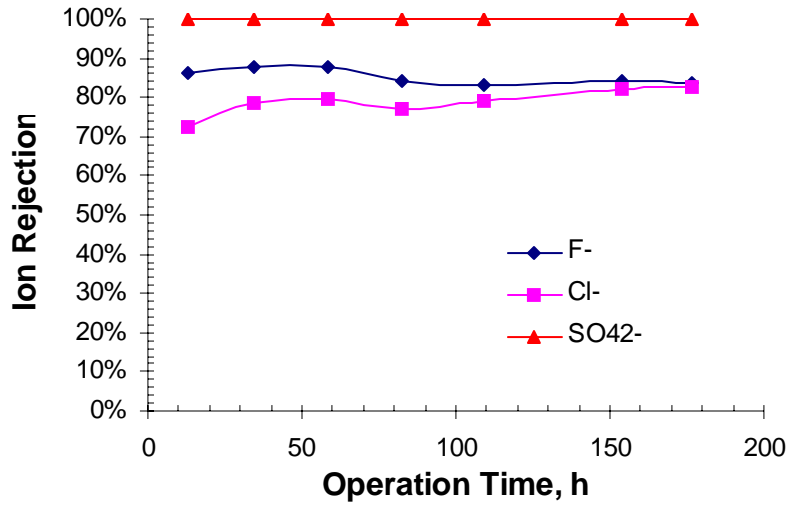


**Fig. 4-2.** Anion rejection as a function of operation time for the gasfield produced water.

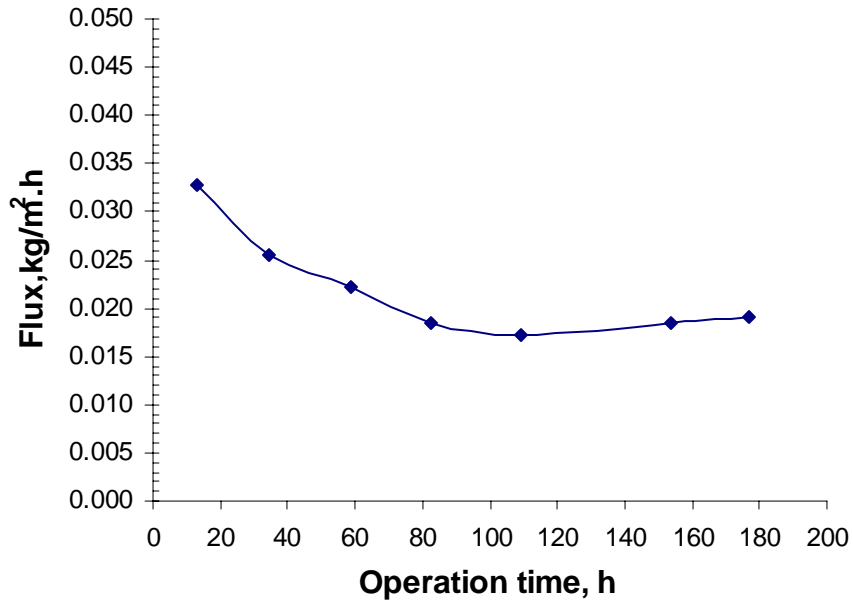


**Fig. 4-3.** Water flux as a function of operation time for the gasfield produced water.

#### 4.1.2 Desalination of Oilfield Produced Water from Hobbs, New Mexico

Figure 4-4 presents cation rejection for the oilfield produced water as a function of operation time. The rejection of  $\text{Ca}^{2+}$  and  $\text{Mg}^{2+}$  ions was as high as 54~57% and rejection of  $\text{Na}^+$  and  $\text{K}^+$  was about 14~15%. The anion rejection was consistent with the rejection of cations, Fig. 4-5. The water flux was about 20% lower than that for the gasfield produced water, Fig. 4-6. The drastically decreased ion rejection compared to the gasfield produced water was caused by the extremely high concentration (>182,000ppm) of salt dissolved in the oilfield produced water, which was ten times that of the gasfield produced water (~18,300ppm). As discussed before, the extremely high ion concentration disables the separation function of the intercrystal micropores (microdefects) in the zeolite membrane. We plan to investigate a few new technologies that can effectively reduce the intercrystal microporous defects, and thus, maintain a high rejection for the produced water with extremely high salt concentrations.

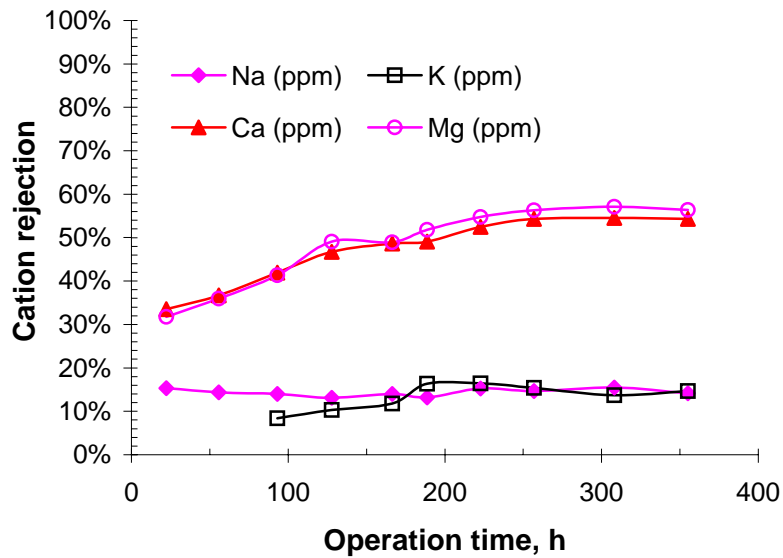


**Fig. 4-4.** Cation rejection as a function of operation time for the oilfield produced water.

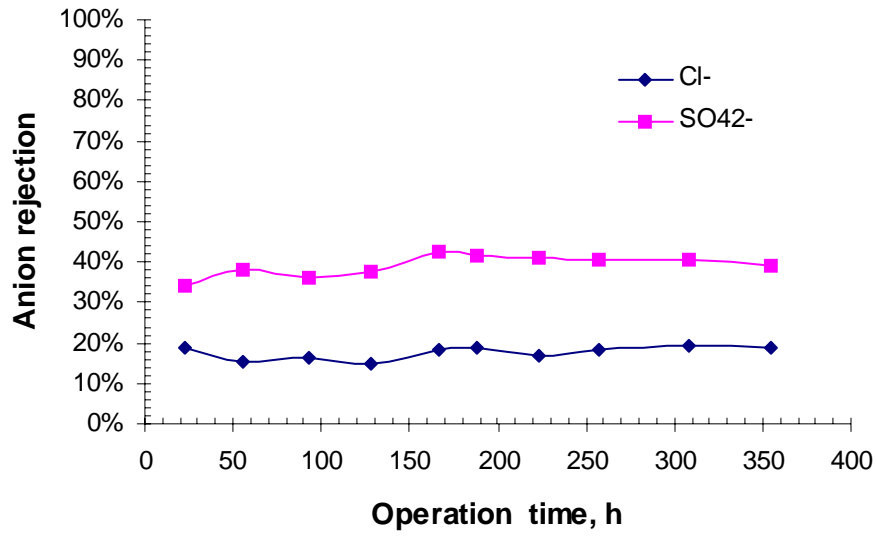


Fig. 4-5. Anion rejection as a function of operation time for the oilfield produced water.

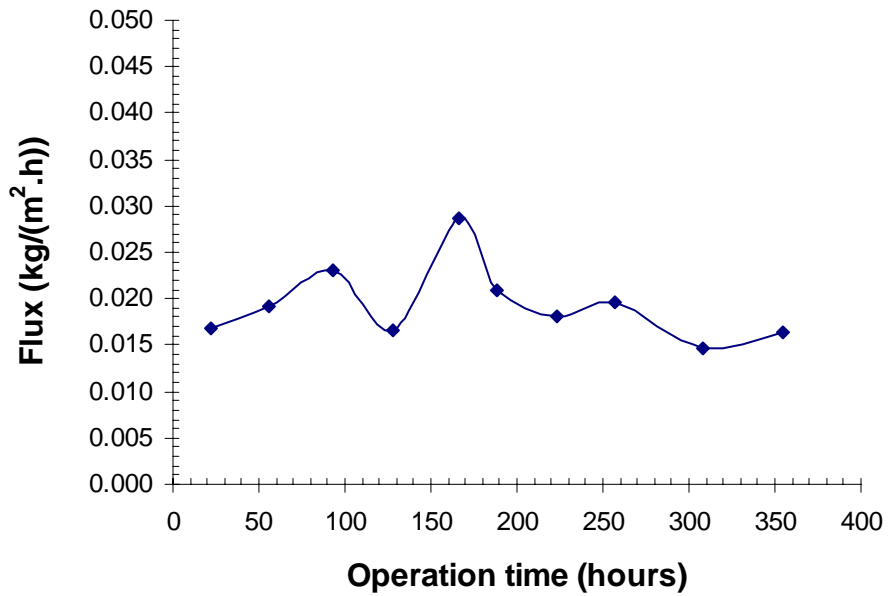


Fig. 4-6. Water flux as a function of operation time for the oilfield produced water.

## CHAPTER 5

### A Novel $\alpha$ -Alumina-Supported Pt-Co/NaY Catalytic Membrane to Overcome the Two-Step Limitation for the Nonoxidative Conversion of Methane

In this study, a  $\alpha$ -alumina-supported Pt-Co/NaY catalytic membrane was developed and demonstrated for overcoming the two-step limitation of nonoxidative CH<sub>4</sub> conversion to higher hydrocarbons (C<sub>2+</sub>) and hydrogen (H<sub>2</sub>). During isothermal operation at 250°C, CH<sub>4</sub> and H<sub>2</sub> were introduced to the feed side and sweep side, respectively, of the membrane. C<sub>2+</sub> formed continuously on the H<sub>2</sub> sweep side while a much smaller quantity of C<sub>2+</sub> was found on the CH<sub>4</sub> feed side. Under the tested conditions, only C<sub>2</sub>H<sub>6</sub> and C<sub>3</sub>H<sub>8</sub> were found in the products on the Pt-Co/NaY membrane and C<sub>2</sub>H<sub>6</sub> was the only detectable product when steady state was reached. A five-step mechanism was proposed based on experimental observations for an ideal membrane process, including:

- (1) Adsorption of CH<sub>4</sub> molecules on the Pt-Co/zeolite surface at the feed side,
- (2) Methane decomposition into carbonaceous species and hydrogen,
- (3) Surface diffusion of chemisorbed carbonaceous species through the zeolite channels to the H<sub>2</sub> sweep side,
- (4) Rehydrogenation of the chemisorbed carbonaceous species to form C<sub>2+</sub> under H<sub>2</sub> sweep, and
- (5) Release of C<sub>2+</sub> into the sweep flow.

#### 5.1 Introduction

Bulk direct dehydrogenation of methane under oxygen-free conditions is thermodynamically unfavorable due to the large positive change in the Gibbs free energy of the reaction. The transition metal-catalyzed nonoxidative CH<sub>4</sub> conversion to higher hydrocarbons (C<sub>2+</sub>) and H<sub>2</sub> has recently attracted much attention<sup>[5-1-3]</sup> because of its outstanding advantages of low reaction temperature, high selectivity, and zero CO<sub>2</sub>-emission. However, practical consideration of the nonoxidative system has been discouraged by

the inherent limitation of its two-step reaction, which requires inefficient discontinuous operations in conventional reactors.

Nonoxidative CH<sub>4</sub> conversion over the transition metal surface consists of two consecutive steps. In the first step, methane is chemisorbed and decomposed into methyl radicals (CH<sub>x(0≤x≤3)</sub>) and hydrogen on the metal surface; in the second step, the chemisorbed carbonaceous radicals are rehydrogenated and oligomerized into C<sub>2+</sub>. The specific form of the chemisorbed species and the mechanism and products of the rehydrogenation/oligomerization step depends on the type of metal catalyst and operational conditions<sup>[5-4-7]</sup>. A relatively high temperature and a high concentration of methane are needed to favor CH<sub>4</sub> chemisorption, while a low temperature and a hydrogen sweep are required to favor the hydrogenation of CH<sub>x(0≤x≤3)</sub> into C<sub>2+</sub>. The two-step nonoxidative CH<sub>4</sub> conversion can be accomplished by either dual-temperature (DT)<sup>[5-4]</sup> or isothermal (IT)<sup>[5-5,6]</sup> operations. For both DT and IT operations, the two steps must be conducted in different atmospheres, the first step in CH<sub>4</sub> and the second step in H<sub>2</sub>. Therefore, inefficient discontinuous operations have to be used to switch the atmosphere in conventional reactors. An extensive review on the surface science and reaction equilibrium and kinetics studies regarding the nonoxidative methane activation has been provided by Choudhary et al.<sup>[5-8]</sup>

Guczi and coworkers<sup>[5-9-11]</sup> reported that Pt-Co/NaY bimetallic catalysts performed better than Pt/NaY and Co/NaY single metal catalysts in terms of surface capacity of methane chemisorption. The Pt-Co/NaY catalyst exhibited 100% conversion of the chemisorbed CH<sub>x</sub> with C<sub>2+</sub> selectivity of 83.6% in the hydrogenation step. The enhanced performance of the Pt-Co/NaY bimetallic catalysts was attributed to the increased reducibility of Co ions in NaY and the synergistic effect of Pt-Co on the C-C bond formation during rehydrogenation<sup>[5-11]</sup>. More recently, they employed a pulse-feeding method on a Pt-Co/NaY fixed-bed reactor for isothermal operation at 250°C<sup>[5-12, 13]</sup>. A significant enhancement of methane conversion was achieved in the pulse-feeding operation compared to the discontinuous operation of switching the gas phase. However, the pulse-feeding, isothermal operation actually performed the two reaction steps separately in time, resulting in a low efficiency of catalyst utilization.

In this study, a Pt-Co/NaY membrane was synthesized on porous  $\alpha$ -alumina substrate where reactants and products flow continuously through the membrane, thereby overcoming the two-step limitation of the nonoxidative methane conversion. The catalytic membrane was tested for continuous, single-step operation of CH<sub>4</sub> conversion at a fixed low temperature of 250°C. This temperature was chosen because catalyst deactivation has been shown to be at a minimum<sup>[5-5,14]</sup>.

## 5.2 Experimental

### 5.2.1 Membrane Synthesis and Characterization

The following chemicals and gases were used in this study: water glass (27%SiO<sub>2</sub>+14%NaOH, Aldrich), sodium aluminate (50-56%Al+40-45%Na (Fe<0.05%), Riedel-deHaen), sodium hydroxide (99.99%, Aldrich), tetraamineplatinum (II) nitrate (50.4%Pt, Aldrich), cobalt (II) nitrate hexahydrate (99.999%, Aldrich), methane (UHP, 99.999%, Matheson Tri Gas), helium (UHP, 99.999%, Matheson Tri Gas), and hydrogen (UHP, 99.999%, Matheson Tri Gas).

NaY zeolite membranes were synthesized on homemade  $\alpha$ -alumina discs by a seeding-secondary growth approach<sup>[5-15]</sup>. The alumina discs were 2 mm thick and 28.6 mm in diameter with a mean pore size of about 0.15 $\mu$ m and a porosity of 35-40%. Both the seed and secondary growth synthesis solutions had a molar composition of 1.0Al<sub>2</sub>O<sub>3</sub>-12.8SiO<sub>2</sub>-17.0Na<sub>2</sub>O-864.2H<sub>2</sub>O. The seeded substrates were hydrothermally treated at 90°C for 24 hours. After hydrothermal synthesis, the membranes were rinsed thoroughly with deionized water to remove the remaining reactants. The membranes were then dried at 50°C in air for two days.

The dry NaY membranes were loaded with metal catalysts by successive ion-exchange followed by calcination and reduction processes. The synthesis procedure included the following basic steps: (1) Pt<sup>2+</sup> ion exchanged by soaking the membrane in a 0.065M Pt(NH<sub>3</sub>)<sub>4</sub>(NO<sub>3</sub>)<sub>2</sub> solution under refluxing at 80°C for 24 hours; (2) washing, drying and then calcining the membrane at 400°C in air for three hours; (3)

Co<sup>2+</sup> ion exchange for the calcined membrane in a 0.06M Co(NO<sub>3</sub>)<sub>2</sub> under refluxing at 80°C for 24 hours; (4) washing, drying and calcining the membrane at 400°C in air for three hours. The resultant membrane was mounted in a stainless steel cell sealed with graphite gaskets (MERCER, NJ) and reduced under pure H<sub>2</sub> permeation at 400°C prior to the CH<sub>4</sub> conversion test.

X-ray diffraction (XRD) (Rigaku, Model D/MAX-II) was used to identify the crystal phase of the membranes. The chemical composition of the zeolite phase and the loaded Pt and Co were determined by X-ray fluorescence (XRF) (Phillips PW2400 wavelength dispersive X-ray spectrometer with Rh and window tube controlled by X40 software). Scanning electron microscope (SEM) (JEOL, JSM-5800LV) was used to observe the morphology of the membranes.

### **5.2.2. Membrane Reaction**

The membrane reactor system is shown schematically in Fig. 5-1. The membrane cell was placed in a temperature-programmable furnace. The feed and sweep gases were composed up by pure gases through calibrated gas mass flow controllers (MFC). All the gases flowed through appropriate gas purifiers (Supelco Molecular Sieve 5A trap for methane and Supelpure-O columns for hydrogen and helium) before mixing and entering the membrane reactor. A mass spectrometer (MS) (UTI, Model 100C) was connected to the outlet of the H<sub>2</sub>-sweep side for online monitoring. Liquid nitrogen cold traps were installed in both the feed and sweep outlet lines to collect the C<sub>2+</sub> products, which were analyzed by a HP 5890 (II) gas chromatograph (GC) with a Porapak © Q packed column.

In all the experiments, the membrane surface faced the H<sub>2</sub> sweep and the substrate was on the CH<sub>4</sub> feed side. The membrane was first reduced at 400°C for four hours by flowing pure H<sub>2</sub> on both feed and sweep sides. Then the temperature was reduced to 250°C at 2°C/min. Approximately 30 min after reaching 250°C, the sweep flow was switch to a mixture of H<sub>2</sub>-He with a controlled H<sub>2</sub>/He mole ratio and flow rate and the feed side flow was switched to pure He with a flow rate of 20 cm<sup>3</sup> (STP)/min. CH<sub>4</sub> was then introduced to the feed flow 40 min later to start the conversion experiment.

**Table 5-1.** Chemical Composition of the Pt-Co/NaY Membrane Layer

Element	Mole percent	Component	Weight percent
Si	55.4	SiO <sub>2</sub>	54.1
Al	32.0	[AlO <sub>2</sub> ] <sup>-</sup>	30.7
Pt	3.0	Pt	9.6
Co	3.5	Co	3.4
Na	6.0	Na <sup>+</sup>	2.2
Total	100.0	Total	100.0

**Table 5-2.** C<sub>2+</sub> Formed during the Membrane Regeneration Process

	C <sub>2</sub> H <sub>6</sub> total μmol	C <sub>3</sub> H <sub>8</sub> total μmol	μmol-C <sub>2</sub> H <sub>6</sub> per g-(Pt-Co/NaY)*	μmol-C <sub>3</sub> H <sub>8</sub> per g-(Pt-Co/NaY)*
From He flow				
(Feed side)	0.63x10 <sup>-2</sup>	0.46 x10 <sup>-3</sup>	1.26	0.092
From H <sub>2</sub> flow				
(Sweep side)	1.83 x10 <sup>-2</sup>	1.01 x10 <sup>-3</sup>	3.66	0.202

\* Total amount of Pt-Co/NaY catalyst of the supported membrane was ~ 5 mg as estimated from the membrane thickness.

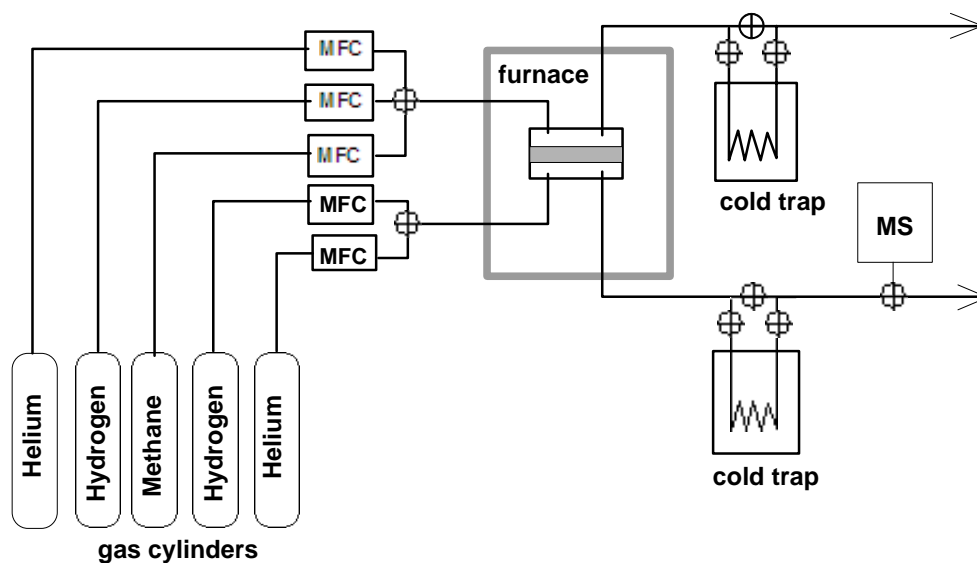
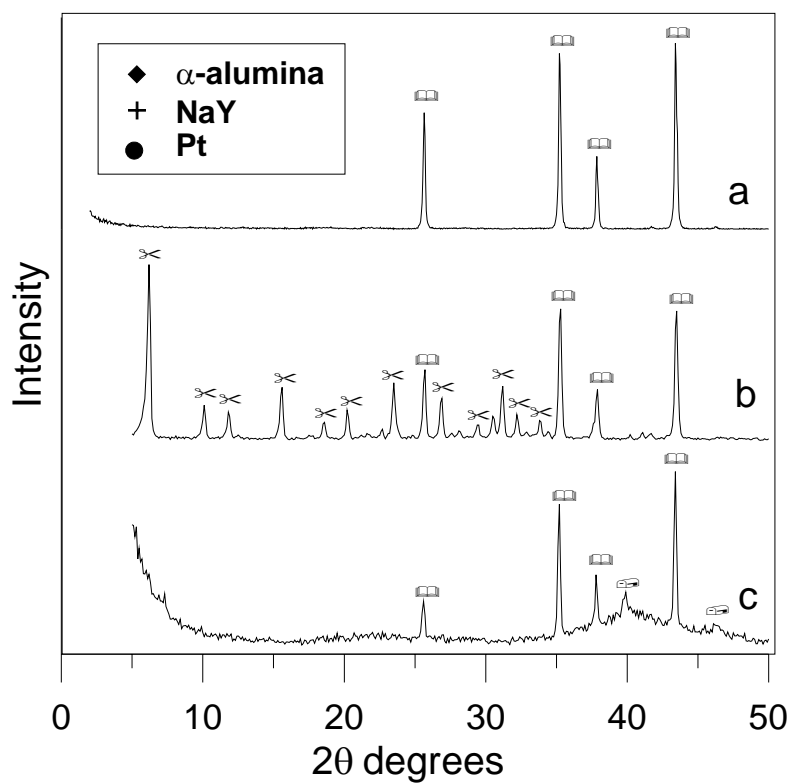


Fig. 5-1. Schematic diagram of the membrane reactor system.

## 5.3 Results

### 5.3.1. The Pt-Co/NaY Membrane

The XRD patterns of the  $\alpha$ -alumina substrate, the NaY membrane, and the Pt-Co/NaY catalytic membrane are given in Fig. 5-2. The XRD patterns revealed that NaY zeolite membrane was obtained without appreciable impurity phases. After loading the Pt-Co catalyst, the NaY peaks were no longer seen in the XRD pattern and no well-defined diffraction peaks of Co were observed. However, the base line developed a broad hump in the  $2\theta$  region of the Pt(111), Pt(200) and Co(111) peaks, suggesting that cobalt existed as highly dispersed atomic clusters. The disappearance of the zeolite XRD peaks on the metal-loaded catalyst has been previously reported in the literature<sup>[5-16]</sup>. A possible reason is the decrease in the zeolite crystallinity and partial crystal structure damage caused by a large degree ion exchange<sup>[5-17]</sup>. The SEM image of the Pt-Co/NaY membrane surface (Fig. 5-3) confirms that the morphology of the zeolite crystals was well preserved after catalyst loading. Figure 5-4 shows the cross-sectional SEM pictures of the plain NaY membrane and the Pt-Co/NaY membrane, each approximately 10 $\mu$ m thick. Metal loading was (0.56mmol-Pt+0.66mmol-Co)/g-NaY as determined by XRF (see Table 5-1).



**Fig. 5-2.** XRD patterns of the substrate and supported NaY and Pt-Co/NaY membranes. (a)  $\alpha$ -alumina substrate, (b) supported NaY membrane, (c) supported Pt-Co/NaY membrane.

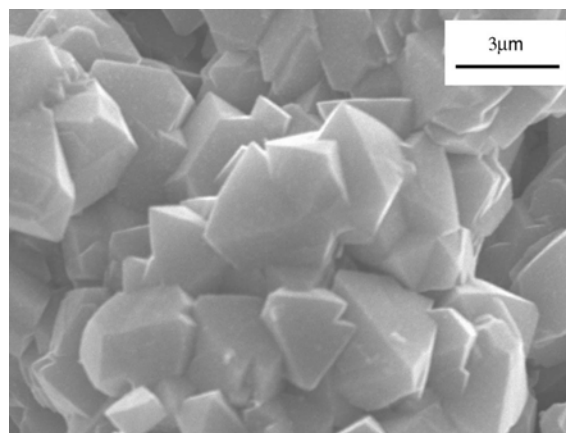
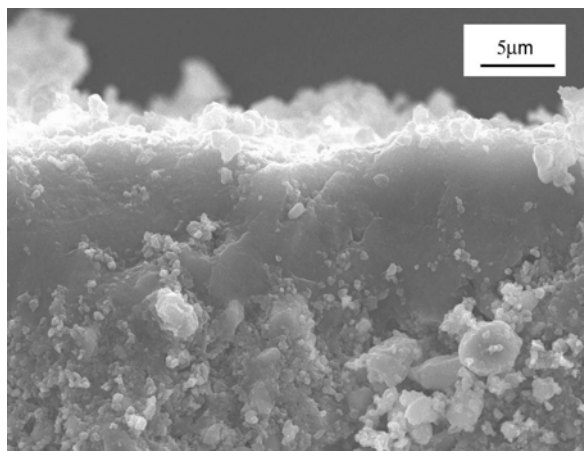
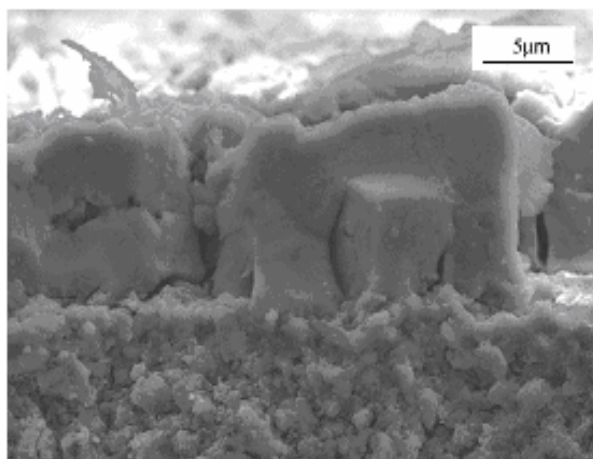


**Fig. 5-3.** Crystal morphology of the Pt-Co/NaY membrane surface.



(a)



(b)

**Fig. 5-4.** Cross-section SEM images of the membranes. (a) NaY membrane, (b) Pt-Co/NaY membrane.

SEM examination showed that some micro-cracks formed in the Pt-Co/NaY membrane probably during the catalyst loading process. The transient N<sub>2</sub> single-gas permeation tests also indicated that the microstructure of the Pt-Co/NaY membrane was somewhat damaged. N<sub>2</sub> permeance values before and after catalyst loading were 10<sup>-8</sup>–10<sup>-7</sup> mol/m<sup>2</sup>·Pa·s and 10<sup>-7</sup>–10<sup>-6</sup> mol/m<sup>2</sup>·Pa·s, respectively. The increase in N<sub>2</sub> permeance after thermal treatment and reduction of the membrane suggests formation of microdefects such as microcracks and enlargement of intercrystal pores caused by zeolite structural change and

mismatch of thermal expansion between the zeolite and alumina substrate<sup>[5-18,19]</sup>. However, the integrity of the membranes remained high enough to continue catalytic studies.

### 5.3.2 Nonoxidative CH<sub>4</sub> Conversion

In all CH<sub>4</sub> conversion experiments, the inlet of the feed side had a constant CH<sub>4</sub>-He total flow rate of 30 cm<sup>3</sup> (STP)/min and CH<sub>4</sub>/He molar ratio of 1:2. The experiments were operated under atmospheric pressure, which was 0.86 bar in the lab (Socorro, New Mexico). A fixed He flow rate of 10 cm<sup>3</sup> (STP)/min was maintained but two different H<sub>2</sub> flow rates were tested in the H<sub>2</sub>-He sweep side inlet. In the first experiment, a H<sub>2</sub> flow rate of 2 cm<sup>3</sup> (STP)/min was used that resulted in a total sweep flow rate of 12 cm<sup>3</sup> (STP)/min and H<sub>2</sub>/He molar ratio of 1:5. In the second experiment, the sweep inlet had a H<sub>2</sub> flow rate of 4 cm<sup>3</sup> (STP)/min that gave a total sweep flow rate of 14 cm<sup>3</sup> (STP)/min and a H<sub>2</sub>/He molar ratio of 1:2.5. The same membrane was used in the two experiments. Between the two experiments, the catalytic membrane was regenerated by flowing pure H<sub>2</sub> on the sweep side and pure He on the feed side at 400 °C for one hour. C<sub>2+</sub> generated in the membrane regeneration process was also collected and analyzed.

In the first experiment with low H<sub>2</sub> concentration in the sweep flow, C<sub>2</sub>H<sub>6</sub> was found to be the only product on both the CH<sub>4</sub> feed side and the H<sub>2</sub> sweep side. No other higher hydrocarbons were detected in the product collected by the cold trap. The reaction was conducted continuously for 90 min at 250°C. Products were analyzed at a typical time interval of 15 min. The results are shown in Fig. 5-5. C<sub>2</sub>H<sub>6</sub> was found in the CH<sub>4</sub>-He feed outlet in the first 15 min but was not detected afterwards. On the H<sub>2</sub>-He sweep side, production of C<sub>2</sub>H<sub>6</sub> was the highest in the first 15 min and then quickly decreased and stabilized at a low value. The CH<sub>4</sub> flux through the membrane was determined to be 2 mmol/m<sup>2</sup>·s by online GC analysis of the permeate stream during the reaction.

After the first conversion test, the membrane was regenerated under conditions similar to those used by Guviz and coworkers for reactivation of Pt-Co/NaY in a packed-bed reactor<sup>[5-13]</sup>. The membrane was first purged with He for four hours at 250°C. Then the temperature was increased to 400°C. At 400°C, the

sweep side was switched to a pure H<sub>2</sub> flow at 6 cm<sup>3</sup> (STP)/min and the feed side maintained a He flow of 20 cm<sup>3</sup> (STP)/min. The He (feed side) and H<sub>2</sub> (sweep side) outlet streams were cold-trapped for 60 min and the products were analyzed. The results are shown in Table 5-2. Both C<sub>2</sub>H<sub>6</sub> and C<sub>3</sub>H<sub>8</sub> were found in the He and H<sub>2</sub> streams. The gas chromatogram also indicated that there might be CH<sub>4</sub> in the regeneration products but the peaks were not well defined for quantitative analysis. It must be noted that capturing the dilute CH<sub>4</sub> under a high flow rate might be difficult because of its low boiling point. No more hydrocarbons were collected from the regeneration streams after 60 min.

After regeneration, the membrane was used directly for the second experiment at 250°C with higher H<sub>2</sub> concentration in the sweep flow. The conversion results on the sweep side are shown in Figure 5-6. In this case, C<sub>2</sub>H<sub>6</sub> and C<sub>3</sub>H<sub>8</sub> were found in the product collected in the first 15 min. However, C<sub>3</sub>H<sub>8</sub> was not detected in the products collected afterwards. Again, the production rate of C<sub>2</sub>H<sub>6</sub> was found to decrease and stabilize at a low level in 30 min. Moreover, C<sub>2</sub>H<sub>6</sub> productivity at steady state was significantly lower compared to that obtained by using a sweep flow with lower H<sub>2</sub> concentration.

To study C<sub>3</sub>H<sub>8</sub> production during the membrane process, the experiment was repeated on a new membrane under the same conditions and online MS was employed to monitor the C<sub>3</sub>H<sub>8</sub> (m/e = 44) in the H<sub>2</sub> sweep outlet. The results are shown in Fig. 5-7 together with that of a reference run on a plain NaY membrane under identical conditions. On the Pt-Co/NaY membrane, a strong response at m/e=44 (corresponding to C<sub>3</sub>H<sub>8</sub> and CO<sub>2</sub>) was found within the first 10 min after introducing CH<sub>4</sub> to the feed. No intensity change at m/e=44 was observed on the plain NaY membrane, indicating that the intensity change at m/e=44 was only caused by C<sub>3</sub>H<sub>8</sub> formed on the catalytic membrane. In addition, analysis by the liquid nitrogen condensation method showed that C<sub>2</sub>H<sub>6</sub>, C<sub>3</sub>H<sub>8</sub>, and other condensable compounds were negligible in all the feed gases (after the purifiers) compared to the amount of C<sub>2+</sub> collected from the membrane reaction.

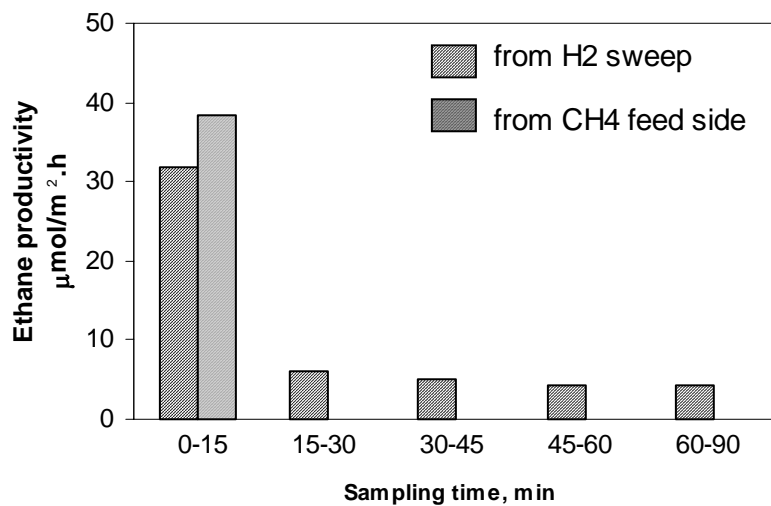


**Fig. 5-5.** C<sub>2</sub>H<sub>6</sub> production rate at the CH<sub>4</sub> feed side and H<sub>2</sub> sweep side as a function of operation time. Sweep flow: 12 cm<sup>3</sup> (STP)/min (H<sub>2</sub>:He = 1:5).

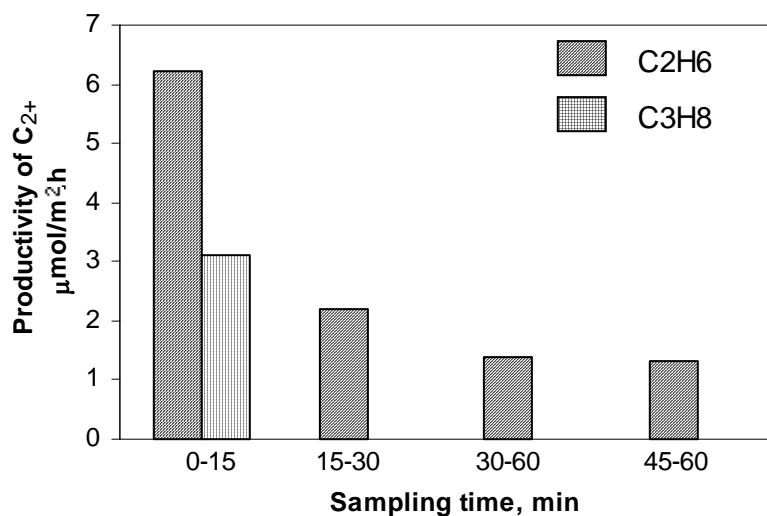


**Fig. 5-6.** C<sub>2+</sub> production rate on the H<sub>2</sub> sweep side as a function of operation time. Sweep flow: 14 cm<sup>3</sup> (STP)/min (H<sub>2</sub>:He = 1:2.5).

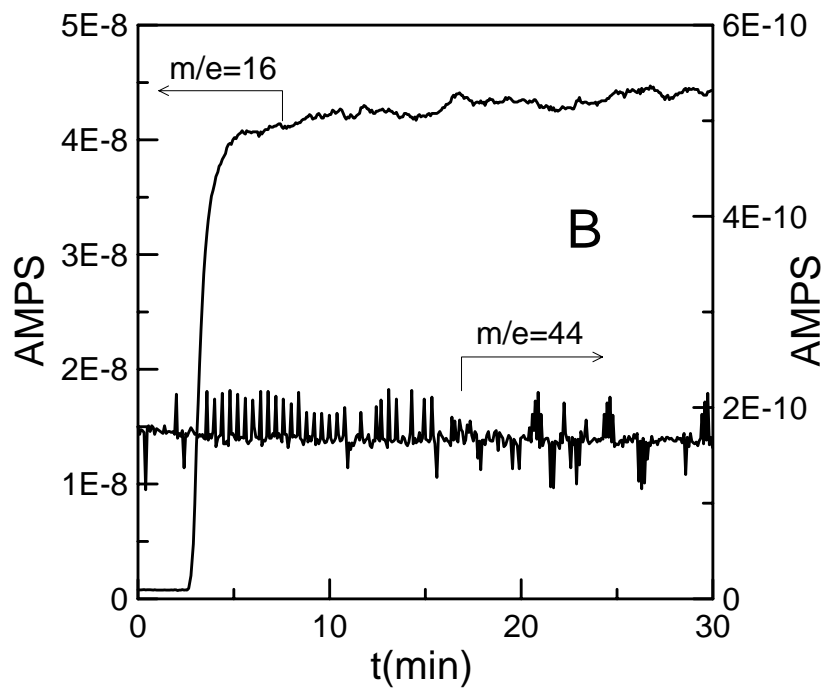
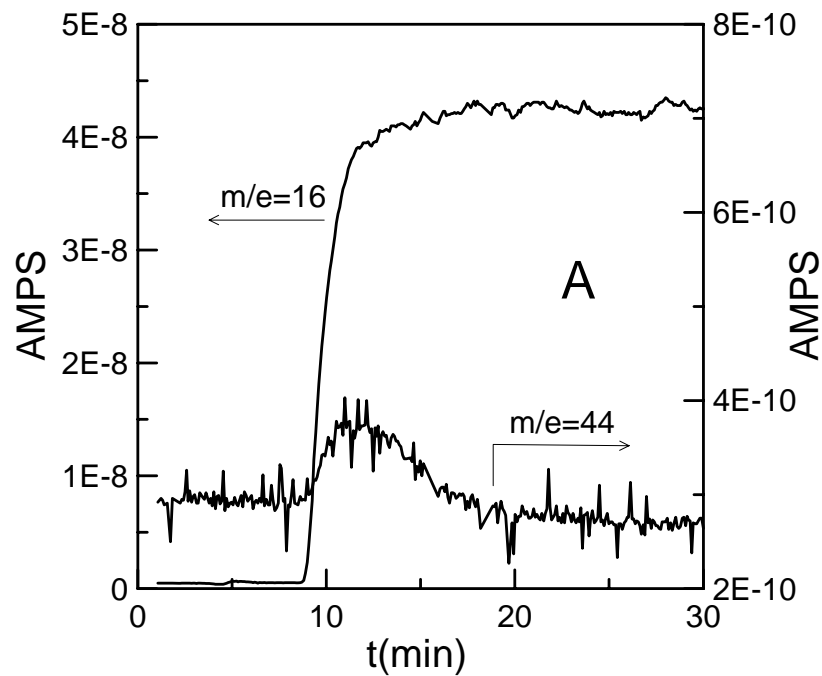


**Fig. 5-7.** MS spectrums of the permeate stream during membrane process at 250°C. A – on Pt-Co/NaY membrane, B – on plain NaY membrane.

## 5.4 Discussion

Although the catalytic membranes contained some microcracks, the experimental results demonstrated that CH<sub>4</sub> conversion occurred through a membrane process. A five-step mechanism is proposed for the nonoxidative CH<sub>4</sub> conversion process on an ideal membrane, which does not allow transfer of molecular CH<sub>4</sub> and H<sub>2</sub> to their counter sides through nonreactive paths.

Step 1: adsorption of CH<sub>4</sub> molecules on metal surface at the feed side of the membrane,

Step 2: methane decomposition into chemisorbed carbonaceous species and hydrogen,

Step 3: surface diffusion of chemisorbed carbonaceous species to the H<sub>2</sub>-sweep side driven by the surface coverage gradient <sup>[5-20]</sup> along the zeolite channels, while the feed stream carries away the generated H<sub>2</sub>,

Step 4: hydrogenation of the chemisorbed carbonaceous species to form C<sub>2+</sub> under H<sub>2</sub> sweep, and

Step 5: release of C<sub>2+</sub> into the sweep flow.

On a real membrane, gaseous CH<sub>4</sub> molecules can diffuse through the zeolite pores and thus CH<sub>4</sub> decomposition may occur anywhere inside the metal-loaded zeolite channels. A certain amount of hydrogen is inevitably present in the zeolite pores as gaseous molecules and chemisorbed protons. This hydrogen comes from the products of CH<sub>4</sub> dehydrogenation as well as back diffusion of the sweep H<sub>2</sub> under partial pressure differences. Therefore, C<sub>2+</sub> might also form inside the zeolitic channels. However, because the effective size of the zeolite channels (0.74 nm dia.) is reduced by the loaded metal clusters and the chemisorbed carbonaceous species, intracrystal gas phase diffusion of CH<sub>4</sub> and H<sub>2</sub> molecules is likely hindered. This supposition is supported by the fact that much less C<sub>2+</sub> was found on the CH<sub>4</sub>-He feed side than on the sweep side at steady state. Since C<sub>2+</sub> molecules can diffuse to both sides if they form inside the channels, the minimal C<sub>2+</sub> on the CH<sub>4</sub> feed side reiterates that the rehydrogenation mainly occurred at or near the surface of the H<sub>2</sub> sweep side.

The radical diffusion process was further evidenced by the results of  $C_{2+}$  production in the membrane reactivation process. During the regeneration process, the chemisorbed carbonaceous species were rehydrogenated into  $C_{2+}$  mainly on the  $H_2$  sweep side while a much smaller amount of  $C_{2+}$  was found in the He flow on the other side. This observation suggests:

- (1) The carbonaceous species may diffuse from the area of higher coverage, namely the original  $CH_4$  feed side, to the area of lower coverage, the original  $H_2$  sweep side, as they are consumed continuously by hydrogenation on the  $H_2$  sweep side.
- (2) On the side of He flow, the small quantity of  $C_{2+}$  was either generated by hydrogenation of carbonaceous species in the presence of  $H_2$  diffused from the other side or from back-diffusion of  $C_{2+}$  formed on the  $H_2$  sweep side or inside the zeolite pores.
- (3) The  $C_{2+}$  production rate obtained on the basis of the one-hour regeneration process was higher than that obtained in the actual conversion process. This was because of the much higher  $H_2$  partial pressure (pure  $H_2$  sweep) and minimized  $CH_4$  (no  $CH_4$  leak from the feed side during membrane regeneration) on the sweep side surface.

The catalytic activity of the membrane, in terms of  $C_{2+}$  production rate, seemed to stabilize after an initial decrease in the first 15 min of operation. The low temperature isothermal operation, coexistence of hydrogen, and enhanced C-C bond formation on the Pt-Co bimetallic surface in NaY, which all favor formation of reactive carbonaceous species ( $C_\alpha$ )<sup>[5-9, 21]</sup>, may be responsible for the minimized deactivation of the catalytic membrane. The radical diffusion process may also influence the activity of the chemisorbed carbonaceous species by affecting its energy profile and the effective  $CH_4$  exposure and aging times<sup>[5-9, 22-24]</sup>.

The  $C_{2+}$  production rate was low, thus yielding low permeate-based  $CH_4$  conversion in the continuous membrane process, compared to the value obtained during the membrane regeneration. Clarification of the causes for the low  $C_{2+}$  productivity requires an understanding of the rate-determining step in the

membrane process, which is being covered in our ongoing investigations. However, the leak of CH<sub>4</sub> and H<sub>2</sub> molecules through microdefects can reduce the conversion in three ways.

First, cracks cause a reduction in the diffusion rate of carbonaceous species. The leaked H<sub>2</sub> on the CH<sub>4</sub> feed side decreases the chemisorption of CH<sub>4</sub>, which in turn decreases the population of the chemisorbed radicals, as well as the driving force for their diffusion. Yet the leaked CH<sub>4</sub> increases CH<sub>4</sub> partial pressure on the H<sub>2</sub> sweep side surface that lowers the efficiency of H<sub>2</sub> sweep and oligomerization of the CH<sub>x</sub> radicals. Second, the surface occupation and counter-diffusion of protons in the zeolite channels might further reduce the surface coverage of CH<sub>x</sub> and block its surface migration. Third, the high flux of CH<sub>4</sub> through the nonreactive paths, mainly microcracks, increases the denominator in the expression of CH<sub>4</sub> conversion.

The dominance of C<sub>2</sub>H<sub>6</sub> in the products and the appearance of C<sub>3</sub>H<sub>8</sub> are expected since many researchers have reported similar results on particulate catalysts under similar operation conditions<sup>[5-13,25,26]</sup>. A number of possible causes for the decrease in C<sub>2+</sub> productivity in the second test after membrane regeneration are being investigated and will be reported on in the future. Our theory includes: the increased H<sub>2</sub> partial pressure in the sweep increases the H<sub>2</sub> back diffusion; the increase in microcracks may be created during the thermal cycle of the reactivation; and some nonreactive C<sub>γ</sub> or less reactive C<sub>β</sub> carbon phases form during the heating step of the regeneration process<sup>[5-4,7]</sup> as well as contamination of the metal surface by trace impurities in the gases.

## 5.5 Conclusions

A new class of metal-loaded zeolite membrane has been developed to overcome the two-step limitation of the nonoxidative CH<sub>4</sub> conversion. For the first time, a truly continuous, single-step IT operation was achieved for two-step nonoxidative CH<sub>4</sub> conversion on a Pt-Co/NaY membrane. The C<sub>2+</sub> production rate and permeate-based CH<sub>4</sub> conversion were evident, though low. The significant “leak” of

CH<sub>4</sub> and H<sub>2</sub> molecules to their counter sides is considered an important cause of the low conversion. However, continued research on the rate-determining step of the membrane process, the forms of the chemisorbed species and their surface diffusivities and energy characteristics, and surface reaction kinetics are required for a better understanding of the membrane performance. These fundamental issues will be significantly different in the continuous membranes process as compared to the conventional equilibrium-based batch operation of the two-step reaction. Although much improvement of the membrane is needed, the preliminary results of this research may open up new opportunities for utilization of the advantageous nonoxidative path for CH<sub>4</sub> conversion.

## 5.6 References

- [5-1] Belgued, M., Paréja, P., Amariglio, A., and Amariglio, H.: "Conversion of Methane into Higher Hydrocarbons on Platinum," *Nature* (1991) **352**, 789.
- [5-2] Koerts, T. and Vansanten, R.A.: "A Low Temperature Reaction Sequence for Methane Conversion," *J. Chem. Soc. Chem. Commun.* (1991) 1281.
- [5-3] Amariglio, H., Saint-Just, J. and Amariglio, A.: "Homologation of Methane under Non-Oxidative Conditions," *Fuel Process Technol.* (1995) **42**, 291.
- [5-4] Koerts, T., Deelen, M.J.A.G. and van Santen, R.A.: "Hydrocarbon Formation from Methane by a Low-Temperature 2-Step Reaction Sequence," *J. Catal.* (1992) **138**, 101.
- [5-5] Belgued, M., Amariglio, A., Paréja, P., and Amariglio, H.: "Oxygen-Free Conversion of Methane to Higher Alkanes through an Isothermal Two-Step Reaction on Platinum (EUROPT-1). 1. Chemisorption of Methane," *J. Catal.* (1996) **159**, 441.
- [5-6] Hlavathy, Z., Paál, Z., and Tétényi, P.: "Oxygen-Free Conversion of Methane to Higher Alkanes through an Isothermal Two-Step Reaction on Platinum (EUROPT-1). 1. - Comment," *J. Catal.* (1997) **166**, 118.

- [5-7] Wu, M.C. and Goodman, D.W.: "High-Resolution Electron Energy-Loss Studies of Hydrocarbon Formation from Methane Decomposition on Ru(0001) and Ru(11 $\bar{2}$ 0) Catalysts," *J. Am. Chem. Soc.* (1994) **116**, 1364.
- [5-8] Choudhary, T.V., Aksoylu, E., and Goodman, D.W.: "Nonoxidative Activation of Methane," *Catal. Rev.* (2003) **45**, 151.
- [5-9] Guzzi, L., Van Santen, R. A., and Sarma, K.V.: "Low-Temperature Coupling of Methane," *Catal. Rev.* (1996) **38**, 249.
- [5-10] Guzzi, L., Sarma, K.V., and Borko, L.: "Non-Oxidative Methane Coupling over Co-Pt/NaY Bimetallic Catalysts," *Catal. Lett.* (1996) **39**, 43.
- [5-11] Lu, G., Hoffer, T., and Guzzi, L.: "Reducibility and Co Hydrogenation over Pt and Pt-Co Bimetallic Catalysts Encaged in NaY-zeolite," *Catal. Lett.* (1992) **14**, 207.
- [5-12] Guzzi, L., Borkó, L., Koppány, Zs, and Kiricsi, L.: "'One-Step' Methane Conversion under Nonoxidative Conditions over Pt-Co/NaY Catalysts at Low Temperature," *Stud. Surf. Sci. Catal.* (1998) **119**, 295.
- [5-13] Guzzi, L. and Borkó, L.: "Comparative Study on Hydrogen-Assisted 'One-Step' Methane Conversion over Pd-Co/SiO<sub>2</sub> and Pt-Co/NaY catalysts," *Catal. Today* (2001) **64**, 91.
- [5-14] Garnier, O., Shu, J., and Grandjean, B.P.A.: "Membrane-Assisted Two-Step Process for Methane Conversion into Hydrogen and Higher Hydrocarbons," *Ind. Eng. Chem. Res.* (1997) **36**, 553.
- [5-15] K. Kusakabe, K., Kuroda, T., and Morooka, S.: "Separation of Carbon Dioxide from Nitrogen Using Ion-Exchanged Faujasite-Type Zeolite Membranes Formed on Porous Support Tubes," *J. Membr. Sci.* (1998) **148**, 13.

- [5-16] Imre, B., Hannus, I., Kónya, Z., and Kiricsi, I: "IR Spectroscopic Reinvestigation of the Generation of Acid Sites in Pt-Containing Faujasite Zeolites," *J. Mol. Structure* (2003) **651-653**, 191.
- [5-17] Sato, K., et al.: "Structural Changes of Y Zeolites during Ion Exchange Treatment: Effects of Si/Al Ratio of the Starting NaY," *Micropor. Mesopor. Mat.* (2003) **59**, 113.
- [5-18] Dong, J. et al.: "Template-Removal-Associated Microstructural Development of Porous-Ceramic-Supported MFI Zeolite Membranes," *Micropor. Mesopor. Mat.* (2000) **34**, 241.
- [5-19] Attfield, M.P., and Sleight, A.W.: "Strong Negative Thermal Expansion in Siliceous Faujasite," *J. Chem. Soc. Chem. Commun.* (1998) 601.
- [5-20] Briner, B.G., Doering, M., Rust, H.P., and Bradshaw, A.M.: "Microscopic Molecular Diffusion Enhanced by Adsorbate Interactions," *Science* (1997) **278**, 257.
- [5-21] Belgued, M. et al: "Oxygen-Free Conversion of Methane to Higher Alkanes through an Isothermal Two-Step Reaction on Ruthenium," *J. Catal.* (1996) **161**, 282.
- [5-22] Amariglio, A., Paréja, P., Belgued, M., and Amariglio, H.: "Possibility of Obtaining Appreciable Yields in Methane Homologation through a 2-Step Reaction at 250 °C on a Platinum Catalyst," *J. Chem. Soc. Chem. Commun.* (1994) 561.
- [5-23] Paréja, P., Amariglio, A., Belgued, M., and Amariglio, H.: "Increasing the Yield in Methane Homologation through an Isothermal 2-Reaction Sequence at 250 °C on Platinum," *Catal. Today* (1994) **21**, 423.
- [5-24] Amariglio, H., Paréja, P., and Amariglia, A.: "Carbon Monoxide-Induced Desorption of Alkanes and Alkenes up to C8 after Chemisorption of Methane on Platinum," *Catal. Lett.* (1995) **31**, 19.

[5-25] Solymosi, F., Erdohelyi, A., Cserenyi, J., and Felvegi, A.: “Decomposition of CH<sub>4</sub> over Supported Pd Catalysts,” *J. Catal.* (1994) **147**, 272.

[5-26] Lu, Y., Li, J., and Lin, J.: “Two-Step, Oxygen-Free Conversion of Methane over Supported NiB Amorphous Alloy Catalysts,” *Catal. Lett.* (2001) **76**, 167.